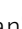






Maternal circulating miRNAs that predict infant FASD outcomes influence placental maturation

Alexander M Tseng¹, Amanda H Mahnke¹ , Alan B Wells^{2,3}, Nihal A Salem¹, Andrea M Allan⁴, Victoria HJ Roberts⁵, Natali Newman⁶, Nicole AR Walter⁶, Christopher D Kroenke⁶, Kathleen A Grant⁶ , Lisa K Akison⁷, Karen M Moritz⁷, Christina D Chambers^{2,3}, Rajesh C Miranda¹ , Collaborative Initiative on Fetal Alcohol Spectrum Disorders

Prenatal alcohol exposure (PAE), like other pregnancy complications, can result in placental insufficiency and fetal growth restriction, although the linking causal mechanisms are unclear. We previously identified 11 gestationally elevated maternal circulating miRNAs (HEA miRNAs) that predicted infant growth deficits following PAE. Here, we investigated whether these HEA miRNAs contribute to the pathology of PAE, by inhibiting trophoblast epithelial-mesenchymal transition (EMT), a pathway critical for placental development. We now report for the first time that PAE inhibits expression of placental pro-EMT pathway members in both rodents and primates, and that HEA miRNAs collectively, but not individually, mediate placental EMT inhibition. HEA miRNAs collectively, but not individually, also inhibited cell proliferation and the EMT pathway in cultured trophoblasts, while inducing cell stress, and following trophoblast syncytialization, aberrant endocrine maturation. Moreover, a single intravascular administration of the pooled murine-expressed HEA miRNAs, to pregnant mice, decreased placental and fetal growth and inhibited the expression of pro-EMT transcripts in the placenta. Our data suggest that HEA miRNAs collectively interfere with placental development, contributing to the pathology of PAE, and perhaps also, to other causes of fetal growth restriction.

DOI 10.26508/lsa.201800252 | Received 22 November 2018 | Revised 20 February 2019 | Accepted 21 February 2019 | Published online 4 March 2019

Introduction

Prenatal alcohol exposure (PAE) is common (1, 2, 3). Between 1.1% and 5% of school children in the United States are conservatively estimated to have a fetal alcohol spectrum disorder (FASD) (4). Consequently, FASD, due to PAE, is the single largest cause of

developmental disabilities in the United States and worldwide (5) and a comorbid factor in a number of other prevalent developmental neurobehavioral disabilities, including attention deficit/hyperactivity and autism spectrum disorders (6).

PAE can result in decreased body weight, height, and/or head circumference in infants. Consequently, infant growth deficits are a cardinal diagnostic feature for fetal alcohol syndrome (7), which represents the severe end of the FASD continuum. However, although well recognized as a diagnostic feature, the mechanistic linkage between PAE and growth restriction remains unclear. In 2016, as part of our effort to identify maternal diagnostic biomarkers of the effect of PAE, we reported that elevated levels of 11 distinct miRNAs in maternal circulation during the second and third trimesters distinguished infants who were affected by in utero alcohol exposure (heavily exposed affected [HEa]) from those who were apparently unaffected at birth by PAE (heavily exposed unaffected [HEua]) or those who were unexposed (UE) (8). In that study, we predicted, based on bioinformatics analyses, that these HEA miRNAs (MIMAT0004569 [hsa-miR-222-5p], MIMAT0004561 [hsa-miR-187-5p], MIMAT0000687 [hsa-miR-299-3p], MIMAT0004765 [hsa-miR-491-3p], MIMAT0004948 [hsa-miR-885-3p], MIMAT0002842 [hsa-miR-518f-3p], MIMAT0004957 [hsa-miR-760], MIMAT0003880 [hsa-miR-671-5p], MIMAT0001541 [hsa-miR-449a], MIMAT0000265 [hsa-miR-204-5p], and MIMAT0002869 [hsa-miR-519a-3p]) could influence signaling pathways crucial for early development, particularly the epithelial-mesenchymal transition (EMT) pathway.

Placental development involves maturation of cytotrophoblasts at the tips of anchoring villi into invasive extravillous trophoblasts, as well as fusion of cytotrophoblasts into multinucleate, hormone-producing syncytiotrophoblasts (9). Maturation into extravillous trophoblasts, which invade the maternal decidua and remodel the uterine spiral arteries into low-resistance high-flow vessels that enable optimal perfusion for nutrient and waste exchange, requires cytotrophoblasts to undergo EMT (10). Impaired placental EMT, as

¹Department of Neuroscience and Experimental Therapeutics, Texas A&M University Health Science Center, Bryan, TX, USA ²Clinical and Translational Research Institute, University of California San Diego, San Diego, CA, USA ³Department of Pediatrics, University of California San Diego, San Diego, CA, USA ⁴Department of Neurosciences, University of New Mexico, Albuquerque, NM, USA ⁵Division of Reproductive and Developmental Sciences, Oregon National Primate Research Center, Oregon Health & Science University, Portland, OR, USA ⁶Division of Neuroscience, Oregon National Primate Research Center, Oregon Health & Science University, Portland, OR, USA ⁷Child Health Research Centre and School of Biomedical Sciences, The University of Queensland, Brisbane, Australia

Correspondence: miranda@medicine.tamhsc.edu; chchambers@ucsd.edu
Rajesh C Miranda and Christina D Chambers are co-senior authors.

well as orchestration of the opposing mesenchymal–epithelial transition pathway, has been found in conditions resulting from placental malfunction, primarily preeclampsia (11, 12, 13, 14, 15, 16). Although there have been no previous studies directly investigating the effects of PAE on placental EMT, a rodent study demonstrated that PAE, during a broad developmental window, reduced the number of invasive trophoblasts within the mesometrial triangle, a region of the uterine horn directly underlying the decidua (17). Furthermore, both human and rodent studies have found PAE disrupts placental morphology and interferes with cytotrophoblast maturation, as with preeclampsia (18, 19, 20, 21). Disrupted trophoblast maturation, seen in these conditions, is associated with aberrant expression of placental hormones, primarily human chorionic gonadotropin (hCG) (22, 23, 24, 25).

Our study is the first to report that PAE interferes with expression of core placental EMT pathway members. Using rodent and primate models of gestation, as well as complementary miRNA over-expression and knockdown studies in vitro, we also provide evidence that HE_a miRNAs, which predict infant growth deficits due to PAE, collectively but not individually, mediate PAE's effects on placental EMT through their effects on cytotrophoblast maturation and cellular stress. In a mouse model of pregnancy, a single combined exposure to the murine-expressed HE_a miRNAs resulted in placental EMT inhibition and diminished placental and fetal growth. Collectively, these data suggest that elevated HE_a miRNAs may represent an emergent maternal stress response that triggers fetal growth restriction, although subgroups of HE_a miRNAs may compete to protect against the loss of EMT. Moreover, most members of the group of

HE_a miRNAs have also been implicated in other placental insufficiency and growth restriction syndromes, giving rise to the possibility that growth restriction syndromes may share common etiological mediators.

Results

HE_a miRNAs are implicated in placental-associated pathologies

Given our prediction that HE_a miRNAs interfere with signaling pathways governing fetal and placental development (8), we conducted a literature review of reports on HE_a miRNA levels in gestational pathologies caused by poor placentation (26, 27, 28). Surprisingly, placental and plasma levels of 8 of 11 HE_a miRNAs were significantly dysregulated in one or more of these gestational pathologies with expression of the majority of these eight miRNAs altered in both fetal growth restriction and preeclampsia (Fig 1A) (29, 30, 31, 32, 33, 34, 35, 36, 37, 38, 39, 40, 41, 42, 43, 44, 45, 46, 47, 48, 49), both of which are characterized by poor placental invasion (50, 51, 52, 53, 54, 55, 56).

HE_a miRNAs explain variance in infant growth outcomes due to PAE

Given the association of individual HE_a miRNAs with gestational pathologies, we sought to determine if circulating HE_a miRNA levels could explain the variance in sex and gestational age-adjusted neonatal height, weight, and head circumference in our Ukrainian birth cohort, which are growth measures sensitive to in utero

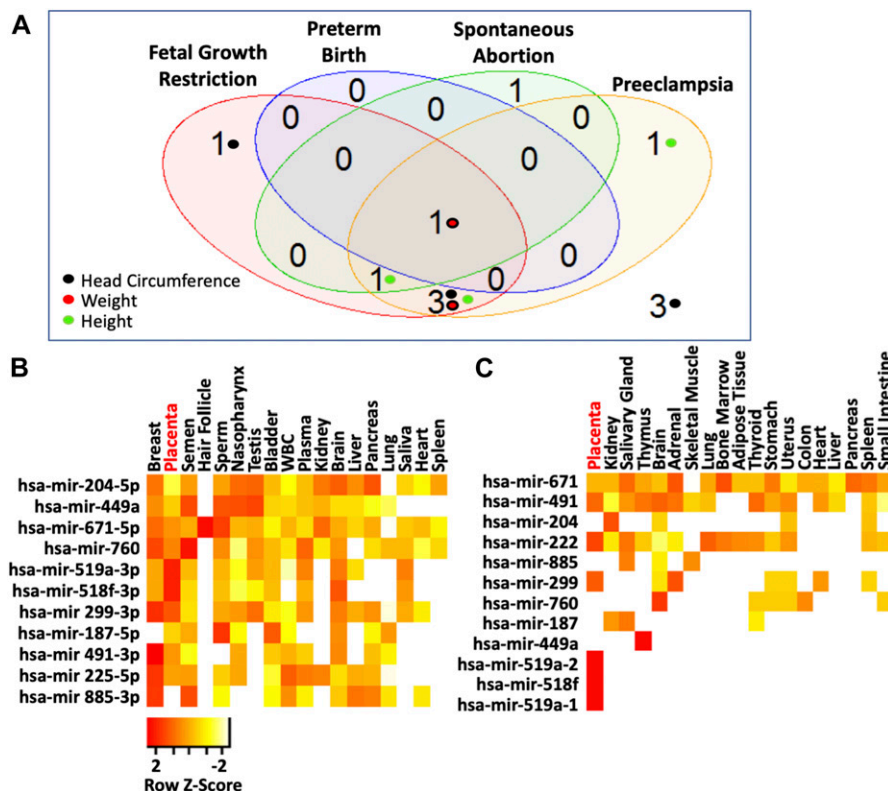


Figure 1. HE_a miRNAs are placentrally enriched and associated with gestational pathologies.

(A) Venn diagram on number of HE_a miRNAs reported to be associated with different gestational pathologies. Inset colored circles represent the corresponding sex and gestational age-adjusted growth parameters these miRNAs were correlated with. Of the 22 studies queried, 11 (50%) used unbiased screenings for miRNA expression. **(B, C)** Heat map of mature HE_a miRNA expression (B) and pri- HE_a miRNA expression (C) across different tissues resulting from secondary analysis of publicly available RNA-sequencing data. Legend depicts row-centered Z-score.

Table 1. $_{\text{HEa}}$ miRNAs are significantly correlated with independent measures of infant size.

MIMAT no.	miRNA	Trimester	Weight			Height			Head circumference		
			Sig.	R ²	ρ	Sig.	R ²	ρ	Sig.	R ²	ρ
MIMAT0004569	hsa-miR-222-5p	2	0.821	1.224	-0.051	0.066	9.572	-0.179	0.8	1.732	-0.104
MIMAT0004561	hsa-miR-187-5p	2	0.462	6.347	0.068	0.17	12.607	-0.074	0.134	10.903	0.103
MIMAT0000687	hsa-miR-299-3p	2	0.552	1.113	0.029	0.069	9.299	-0.203	0.036^a	8.65	0.1
MIMAT0004765	hsa-miR-491-3p	2	0.172	3.61	0.112	0.849	2.033	-0.055	0.024^a	12.529	0.156
MIMAT0004948	hsa-miR-885-3p	2	0.142	4.227	-0.174	0.044^a	7.667	-0.231	0.59	1.36	-0.115
MIMAT0002842	hsa-miR-518f-3p	2	0.246	2.517	0.134	0.918	2.134	-0.118	0.007^b	14.561	0.219
MIMAT0004957	hsa-miR-760	2	0.059	6.314	0.195	0.22	4.096	0.079	0.055	10.158	0.195
MIMAT0003880	hsa-miR-671-5p	2	0.123	7.24	0.11	0.578	5.264	-0.031	0.073	10.794	0.107
MIMAT0001541	hsa-miR-449a	2	0.101	11.584	0.104	0.718	5.851	-0.072	0.173	10.036	0.068
MIMAT0000265	hsa-miR-204-5p	2	0.026^a	12.377	0.184	0.272	4.973	0	0.131	7.095	0.108
MIMAT0002869	hsa-miR-519a-3p	2	0.034^a	7.975	0.153	0.403	6.83	-0.012	0.093	8.181	0.096
MIMAT0004569	hsa-miR-222-5p	3	0.875	0.993	-0.046	0.018^a	10.709	-0.196	0.577	4.696	-0.01
MIMAT0004561	hsa-miR-187-5p	3	0.538	2.055	0.049	0.37	2.029	-0.109	0.784	3.697	0.002
MIMAT0000687	hsa-miR-299-3p	3	0.511	0.762	0.005	0.514	1.769	-0.072	0.87	3.786	-0.077
MIMAT0004765	hsa-miR-491-3p	3	0.824	3.165	-0.028	0.2	12.122	-0.121	0.747	4.188	-0.081
MIMAT0004948	hsa-miR-885-3p	3	0.807	0.148	0.029	0.102	4.686	-0.156	0.376	5.009	0.032
MIMAT0002842	hsa-miR-518f-3p	3	0.515	2.099	0.109	0.421	1.715	0.016	0.245	7.917	0.152
MIMAT0004957	hsa-miR-760	3	0.368	1.396	0.141	0.761	0.716	-0.022	0.207	6.052	0.172
MIMAT0003880	hsa-miR-671-5p	3	0.055	8.715	0.155	0.367	3.521	-0.133	0.076	8.196	0.15
MIMAT0001541	hsa-miR-449a	3	0.995	0.085	-0.06	0.982	0.678	-0.151	0.026^a	12.022	0.135
MIMAT0000265	hsa-miR-204-5p	3	0.019^a	11.872	0.23	0.206	5.589	0.022	0.002^b	18.683	0.319
MIMAT0002869	hsa-miR-519a-3p	3	0.391	2.82	0.043	0.302	5.917	-0.151	0.106	9.286	0.118

The correlation of the second and third trimester maternal plasma $_{\text{HEa}}$ miRNA levels with independent measures of infant size. $_{\text{HEa}}$ miRNAs and their significantly correlated sex and gestational age-adjusted growth parameters appear in bold. R² is expressed as the percentage ($\times 100$) of variance explained.

^aP < 0.05.

^bP < 0.01.

environment (57). We found that eight of the $_{\text{HEa}}$ miRNAs each significantly explained between 7% and 19% of infant variation in these growth measures (Table 1). Furthermore, seven of these miRNAs were also associated with fetal growth restriction and preeclampsia as identified by our literature review (Fig 1A). Interestingly, a multivariate statistical regression model that accounted for levels of all 11 $_{\text{HEa}}$ miRNAs together, explained a far greater proportion of infant variance, between 24% and 31%, in all three growth measures than accounting for them individually (Table S1), suggesting $_{\text{HEa}}$ miRNAs collectively account for the variance in infant growth outcomes.

$_{\text{HEa}}$ miRNAs are transcribed preferentially in the placenta

Data extracted from publicly available gene expression profiling datasets (58) show that $_{\text{HEa}}$ miRNAs and their unprocessed precursor transcripts, $_{\text{HEa}}$ pri-miRNAs, are enriched in placenta compared with other tissues, suggesting that the placenta itself transcribes these miRNAs and may be a significant contributory tissue to maternal circulating $_{\text{HEa}}$ miRNAs (Fig 1B and C). Moreover,

because $_{\text{HEa}}$ miRNAs are also associated with gestational pathologies caused by poor placental invasion, these $_{\text{HEa}}$ miRNAs may also contribute to the placental response to PAE. We, therefore, assessed in rodent and primate models, whether PAE could result in impaired EMT, and if $_{\text{HEa}}$ miRNAs could explain the effects of PAE on placental EMT-associated gene expression.

$_{\text{HEa}}$ miRNAs moderate placental EMT impairment in PAE models

EMT, in trophoblasts, is characterized by the disappearance of epithelial markers such as E-Cadherin and the appearance of mesenchymal markers such as the intermediate filament, vimentin, a process that is controlled by the expression of key mesenchymal determination transcription factors, Snail1 and 2 and TWIST, as extensively described (10, 14, 15, 59, 60, 61, 62). These five markers have been used to assess EMT in a variety of model systems, so our studies used these markers to assess the effects of alcohol and $_{\text{HEa}}$ miRNAs on trophoblast EMT.

In the first analysis, using a murine model of PAE that mimicked moderate to binge-type alcohol consumption throughout early and

mid-pregnancy, we fractionated GD14 placenta into three zones: the cytotrophoblast- and syncytiotrophoblast-rich labyrinth zone, the glycogen- and spongiotrophoblast-rich junctional zone, and the

decidual zone comprising the endometrial contribution to the placenta (Fig 2A). Multivariate analysis of variance (MANOVA) for expression of these five core genes in the EMT pathway within

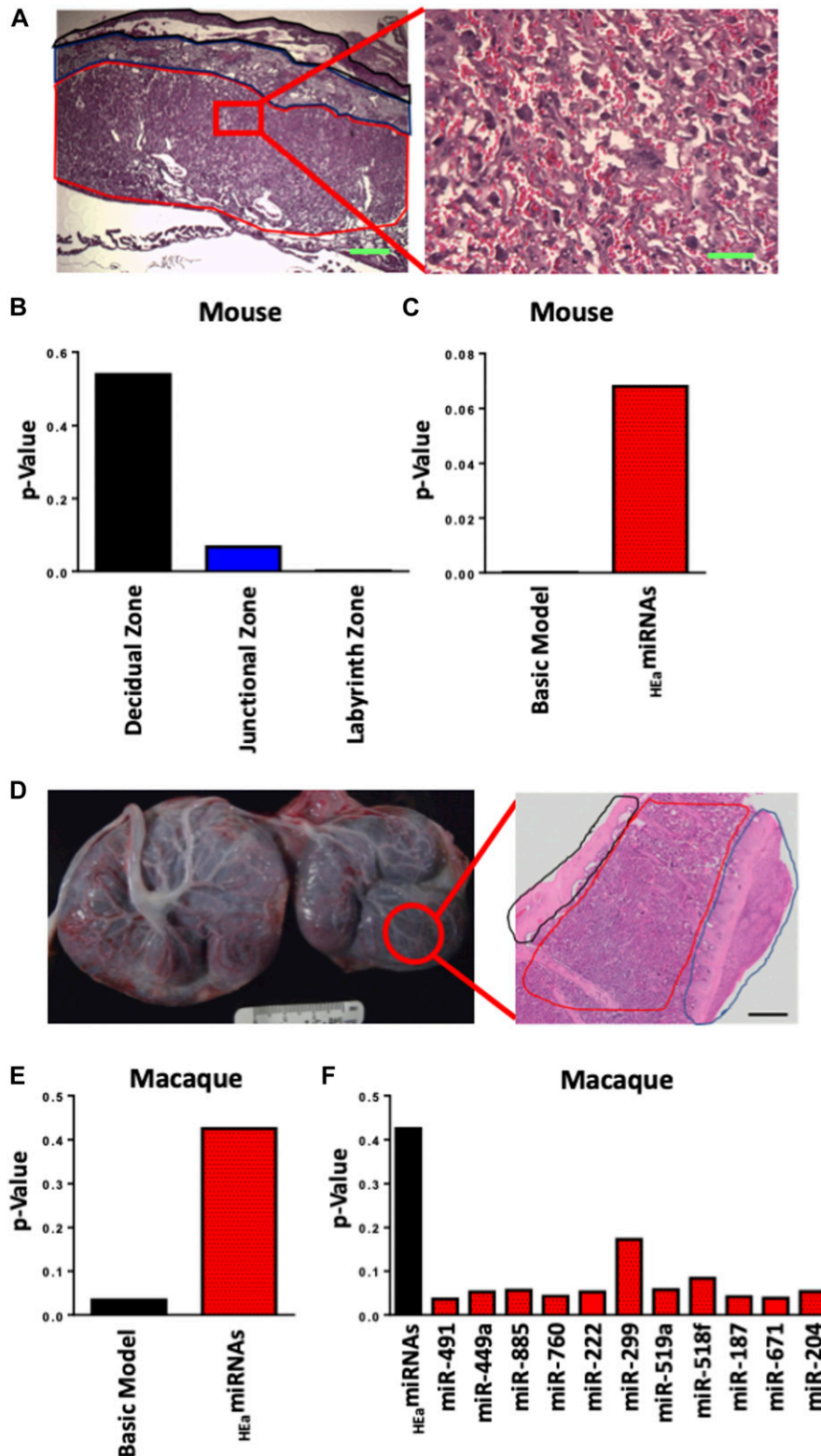


Figure 2. HEa miRNAs mediate the effect of PAE on EMT pathway members in mouse and macaque placentas. **(A)** Histological image of GD14 mouse placenta. Outlined in red is the labyrinth zone, blue is the junctional zone, and black is the decidual zone with the scale bar (green) demarcating 200 μ m. Inset is a high-magnification image of the labyrinth zone with the scale bar (green) demarcating 50 μ m. **(B)** MANOVA of gene expression of core EMT pathway members in different regions of the mouse placenta in control and PAE mice (n = 29 samples). **(C)** MANCOVA of gene expression of core EMT pathway members in the mouse placental labyrinth zone before (Basic Model) and after accounting for the expression of HEa miRNAs (n = 29 samples). **(D)** Gross anatomy photograph of the primary (left) and secondary (right) lobes of a GD135 macaque placenta. Outlined in red is an individual cotyledon from the secondary lobe. Inset is a full thickness hematoxylin and eosin-stained histological section of a representative cotyledon with the fetal membranes outlined in black, villous tissue outlined in red, and maternal decidua in blue. Ruler is 3 cm and scale bar (black) is 2 mm. **(E)** MANCOVA of gene expression of core EMT pathway members in placental cotyledons of PAE and control macaques, accounting for the expression of HEa miRNAs collectively (n = 23 samples). **(F)** MANCOVA of gene expression of core EMT pathway members in macaque placentas after accounting for expression of HEa miRNAs individually (n = 23 samples).

placental trophoblasts revealed a significant effect of ethanol exposure on EMT pathway member expression selectively within the labyrinth zone (Pillai's trace statistic, $F_{(5,21)} = 6.85, P < 0.001$, Fig 2B) but not within the junctional or decidual zones. Post hoc univariate ANOVA indicated ethanol exposure specifically elevated *CDH1* ($F_{(1,25)} = 7.452, P = 0.011$), which encodes epithelial E-Cadherin, whereas expression of the pro-mesenchymal transcription factor *SNAI1*, which encodes Snail1, was significantly reduced ($F_{(1,25)} = 21.022, P = 0.0001$). We also observed a significant interaction between fetal sex and PAE on expression of *SNAI2*, which encodes Snail2 ($F_{(1,25)} = 2.18, P = 0.047$) and a trend towards decreased expression of the terminal

mesenchymal marker *VIM* (vimentin, $F_{(1,25)} = 2.749, P = 0.11$), whereas there was no effect on *TWIST* expression (Fig 3A–E). Consistent with our gene expression data, E-Cadherin protein levels were significantly elevated in the labyrinth zone of PAE placenta ($F_{(1,24)} = 31.63, P = 0.0005$), whereas not in the junctional or decidual zones (Figs 3F and S1A and B). However, when we controlled for expression of the eight mouse homologs of $_{HEa}$ miRNAs as a covariate, using multivariate analysis of covariance (MANCOVA), ethanol's effect on EMT became marginally nonsignificant (Pillai's trace, $F_{(5,21)} = 2.713, P = 0.068$) (Fig 2C), suggesting that these miRNAs partially mediate effects of PAE on EMT pathway members in mice. Interestingly, PAE

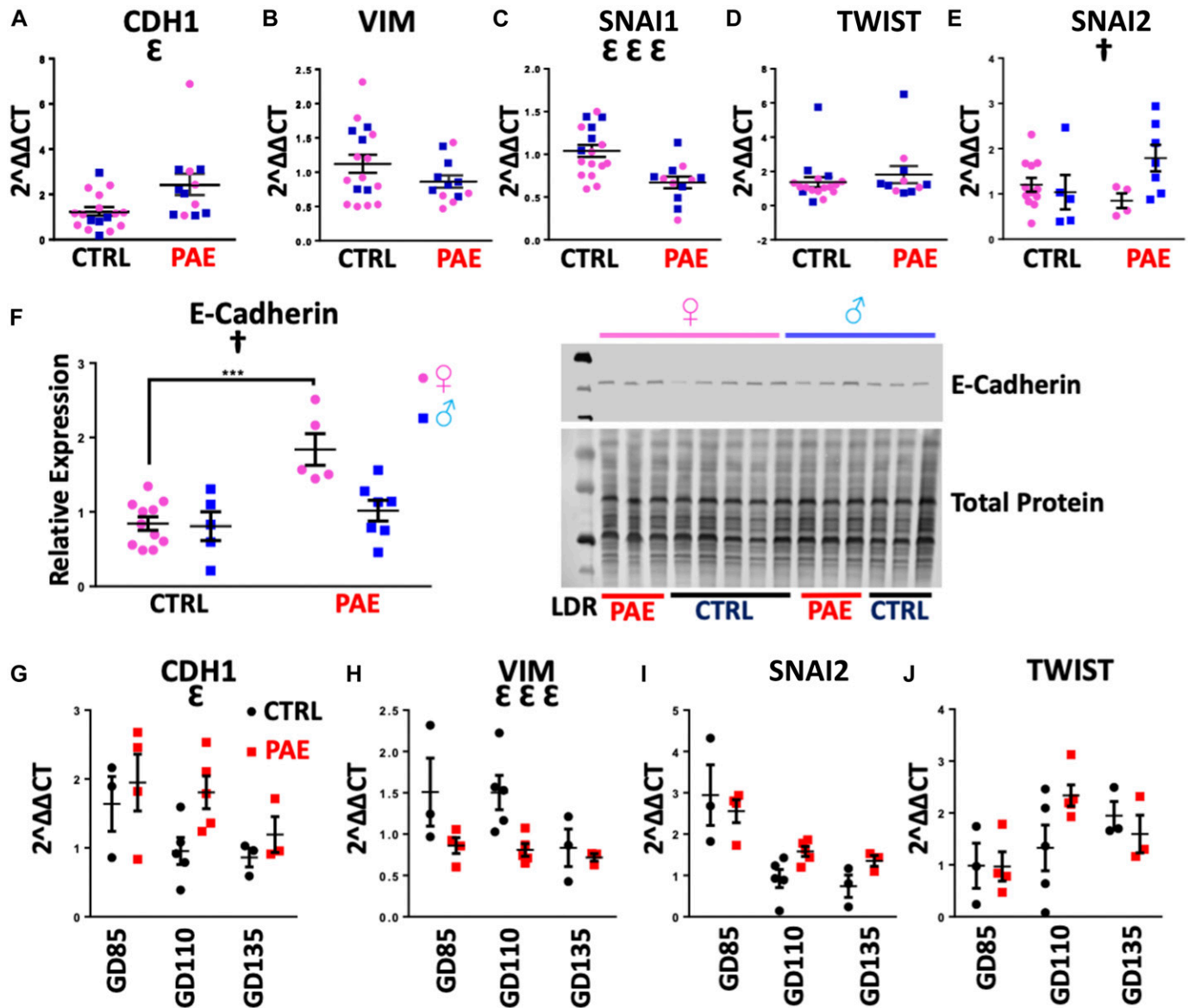


Figure 3. PAE interferes with the EMT pathway in mouse and macaque placentas. (A–E) Expression of *CDH1* (A), *VIM* (B), *SNAI1* (C), *TWIST* (D), and *SNAI2* (E) in the placental labyrinth zone of PAE and control mice ($n = 5$ –12 samples per group). (F) Densitometric quantification of E-Cadherin expression in the labyrinth zone of PAE and control mice as well as representative blot of E-Cadherin expression and total protein expression (right, $n = 5$ –12 samples per group). (G–J) Expression of *CDH1* (G), *VIM* (H), *SNAI2* (I), and *TWIST* (J) transcripts in PAE and control macaque placental cotyledons ($n = 3$ –5 samples per group). Results are expressed as the mean \pm SEM, LDR = molecular weight ladder; ANOVA: significant main effect of PAE ($^{\epsilon}P < 0.05$, $^{\epsilon\epsilon\epsilon}P < 0.001$), significant interaction effect (sex by PAE, $[^{\epsilon}P < 0.05]$). For post hoc analysis, $^{***}P < 0.001$ by Tukey's HSD.

limited to the periconceptional period in rats also influenced expression of EMT core transcripts (Figs S2B and S3A–E).

To determine if PAE's effects on EMT pathway members in placenta are broadly conserved throughout mammalian evolution, we adopted a nonhuman primate (macaque) model of moderate to binge-type alcohol consumption. Placental tissues were isolated from GD85, GD110, and GD135 placenta (Fig 2D), which spans the human equivalent of the mid-second to mid-third trimester (Fig S2C). There was a significant effect of ethanol exposure on expression of core EMT mRNA transcripts by MANOVA (Pillai's trace statistic, $F_{(4,9)} = 4.229$, $P = 0.045$, Fig 3B). Consistent with our findings in mouse, post hoc univariate ANOVA indicated that in primate placenta, ethanol exposure significantly increased *CDH1* expression ($F_{(1,12)} = 4.866$, $P = 0.048$), whereas *VIM* expression was significantly reduced ($F_{(1,12)} = 12.782$, $P = 0.0004$), suggesting that, as in the mouse, PAE also impairs EMT in the primate placenta. Interestingly, there was no effect on *SNAI2* or *TWIST* expression (Fig 3G–J). As in mice, accounting for expression of $_{\text{HEa}}$ miRNAs together as a covariate abolished the significant effect of PAE on EMT, although to a greater degree than mice (Pillai's trace, $F_{(1,1)} = 1.605$, $P = 0.425$, Fig 2E). Interestingly, accounting for expression of individual $_{\text{HEa}}$ miRNAs did not explain the effects of PAE on placental EMT, suggesting that $_{\text{HEa}}$ miRNAs act in concert to mediate the effect of PAE on EMT in the primate placenta (Fig 2F).

Collectively, our data suggest PAE-induced impairment of EMT in the trophoblastic compartment of placentae is conserved between rodents and nonhuman primates and that $_{\text{HEa}}$ miRNAs, particularly in primates, may moderate the effect of PAE on placental EMT. Consequently, subsequent studies focused on the collective role of $_{\text{HEa}}$ miRNAs, either on basal or on alcohol-influenced placental trophoblast growth, invasion, and the maturation of physiological function.

$_{\text{HEa}}$ miRNAs impair EMT in a model of human cytotrophoblasts

To investigate whether $_{\text{HEa}}$ miRNAs collectively interfere with the EMT pathway, as suggested by our in vivo data, we examined the effects of transfecting $_{\text{HEa}}$ miRNA mimics and antagomirs into BeWO cytotrophoblasts (Fig 4A). We initially overexpressed each of the 11 $_{\text{HEa}}$ miRNAs individually, to determine whether any of them could influence the EMT pathway. We did not observe any significant effects (Fig S4), consistent with our findings in the primate PAE model that individual miRNAs did not explain the effects of ethanol on EMT. In contrast, transfection of pooled $_{\text{HEa}}$ miRNAs into cytotrophoblasts significantly increased *CDH1* expression ($F_{(1,36)} = 30.08$, $P < 0.0001$). Interestingly, expression of the pro-mesenchymal transcription factors *TWIST* and *SNAI1* were also significantly reduced, but only in the context of concomitant 320 mg/dl ethanol treatment, pointing to an interaction effect between $_{\text{HEa}}$ miRNAs and ethanol ($F_{(1,36)} = 5.650$ and 5.146 , respectively, $P = 0.023$ and $P = 0.029$, Fig 4B–E). Consistent with our qPCR data, transfection of $_{\text{HEa}}$ miRNAs also significantly increased E-Cadherin protein expression ($F_{(1,20)} = 33.86$, $P < 0.0001$, Fig 4F). We were unable to detect *SNAI2* transcript expression or vimentin protein expression in these cells, consistent with previous reports (63).

We next sought to determine if more restricted subsets of $_{\text{HEa}}$ miRNAs could recapitulate the effects of $_{\text{HEa}}$ miRNAs collectively on EMT. Thus, we overexpressed hsa-miR-222-5p and hsa-miR-519a-3p,

which are implicated in preeclampsia and fetal growth restriction, as well as hsa-miR-885-3p, hsa-miR-518f-3p, and hsa-miR-204-5p, which are implicated in preeclampsia, fetal growth restriction, and spontaneous abortion or preterm labor (Fig S5A). In contrast to the collective action for all $_{\text{HEa}}$ miRNAs, exposure to each of these pools resulted in significant decreases in *CDH1* expression ($F_{(2,12)} = 20.12$, $P = 0.0001$). The pool including hsa-miR-885-3p, hsa-miR-518f-3p, and hsa-miR-204-5p also significantly increased *Snai1* *SNAI1* ($F_{(2,12)} = 4.604$, $P = 0.0328$; Dunnett's post hoc $P = 0.0497$, Fig S5B–E). These data suggest that $_{\text{HEa}}$ miRNAs include subgroups of miRNAs that have the potential to partly mitigate the effects of elevating the entire pool. However, the potential protective effects of these subgroups are masked by the collective function of the entire group of $_{\text{HEa}}$ miRNAs.

Whereas transfection of $_{\text{HEa}}$ miRNA mimics increased *CDH1* expression, transfection of pooled antagomirs to $_{\text{HEa}}$ miRNAs significantly reduced *CDH1* expression, only in the context of 320 mg/dl ethanol co-exposure ($_{\text{HEa}}$ miRNA \times 320 mg/dl EtOH interaction, $F_{(1,36)} = 13.51$, $P = 0.0008$; post hoc Tukey's honest significance difference (HSD), $P = 0.005$, Fig 4G). However, expression of *TWIST* was also decreased with ethanol co-exposure, and there was no significant difference in E-Cadherin protein expression relative to the control (Fig 4H–K). Thus, our data suggest that increasing $_{\text{HEa}}$ miRNA levels impairs EMT pathway members in cytotrophoblasts, whereas inhibiting their action has a more restricted effect on EMT pathway members.

$_{\text{HEa}}$ miRNAs impair EMT in a model of human extravillous trophoblasts

We next investigated the effect of $_{\text{HEa}}$ miRNAs on EMT in HTR-8/SVneo extravillous trophoblast-type cells (Fig 5A). Transfecting pooled $_{\text{HEa}}$ miRNA mimics into extravillous trophoblasts significantly decreased *VIM* expression ($F_{(1,36)} = 28.43$, $P < 0.0001$). Expression of pro-mesenchymal transcription factor *SNAI2* was also reduced ($F_{(1,36)} = 64.88$, $P < 0.0001$). As with cytotrophoblasts, expression of *SNAI1* and *TWIST* were reduced only with 320 mg/dl ethanol co-exposure ($_{\text{HEa}}$ miRNA \times 320 mg/dl EtOH interaction, $F_{(1,36)} = 4.21$ and 5.18 , $P = 0.048$ and 0.029 , respectively; post hoc Tukey's HSD, $P = 0.027$ and $P < 0.0001$, respectively, Fig 5B–E). Consistent with our qPCR data, vimentin protein expression was also significantly reduced ($F_{(1,20)} = 9.535$, $P = 0.006$, Fig 5F). Interestingly, there was also a main effect of alcohol exposure on decreasing vimentin protein expression ($F_{(1,20)} = 7.303$, $P = 0.014$). We were unable to detect expression of *CDH1* transcript, or its E-Cadherin protein product, in extravillous trophoblasts, consistent with previous reports (63).

In contrast to $_{\text{HEa}}$ miRNA mimics, transfecting pooled antagomirs significantly increased *VIM* expression ($F_{(1,35)} = 42.56$, $P < 0.0001$). Likewise, antagomir transfection increased expression of *SNAI2* in the context of 320 mg/dl ethanol co-exposure and *SNAI1* under basal conditions ($_{\text{HEa}}$ miRNA \times 320 mg/dl EtOH interaction, $F_{(1,35)} = 10.31$ and 4.86 , $P = 0.01$ and $P = 0.034$, respectively; post hoc Tukey's HSD, $P < 0.0001$, Fig 5G–J). Despite our qPCR data, we did not observe significant differences in vimentin protein expression between treatment groups (Fig 5K). Collectively, our data indicate that increased trophoblastic $_{\text{HEa}}$ miRNA levels favor an epithelial phenotype, whereas inhibiting their action promotes a mesenchymal phenotype.

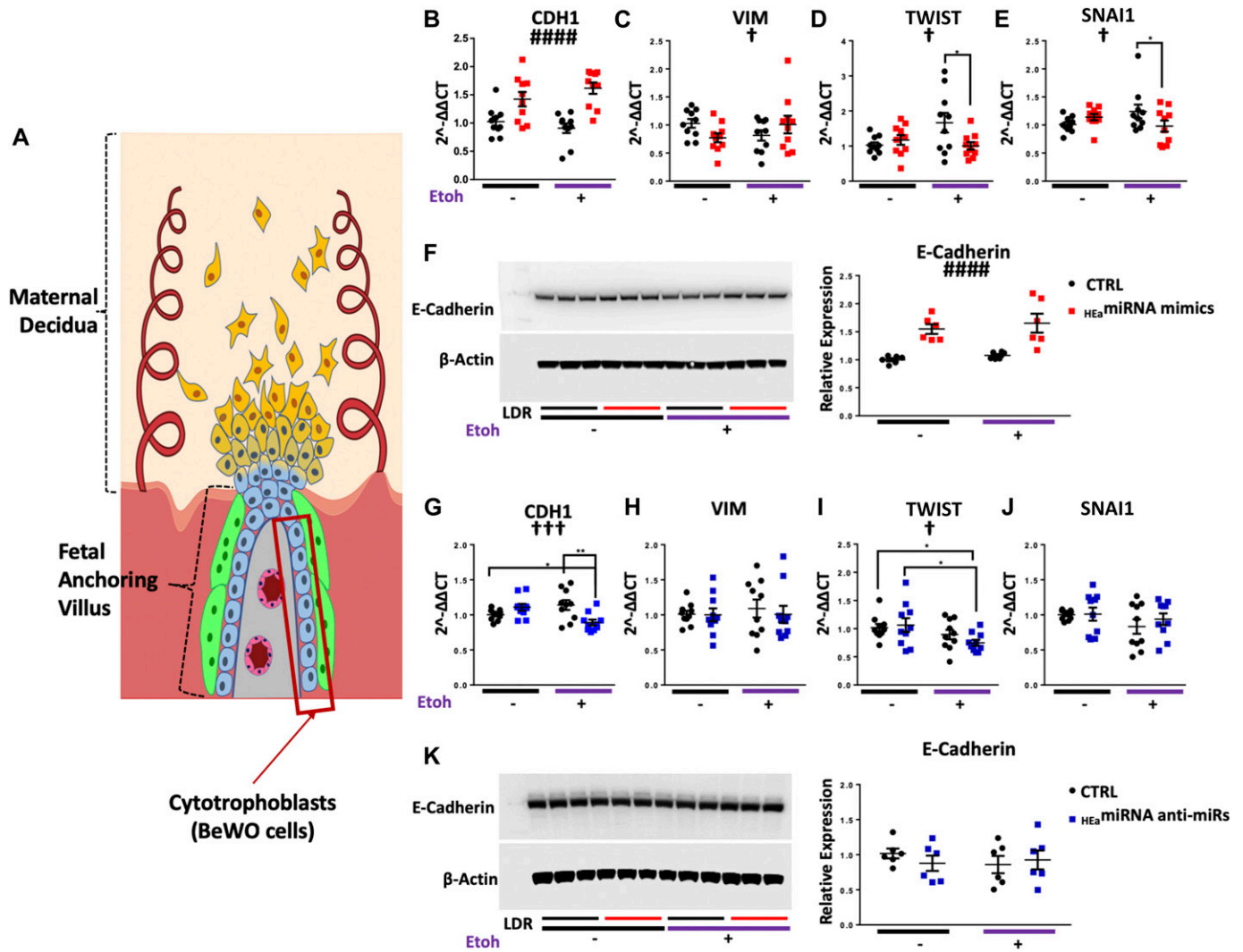


Figure 4. HE_a miRNAs interfere with the EMT pathway in BeWO cytotrophoblasts. (A) Diagram of a placental anchoring villous and maternal decidua with the boxed area denoting cytotrophoblasts. (B–F) Expression of *CDH1* (B), *VIM* (C), *TWIST* (D), and *SNAI1* (E) transcripts and densitometric quantification of E-Cadherin protein levels (F) in BeWO cytotrophoblasts following HE_a miRNA or control miRNA overexpression with or without concomitant 320 mg/dl ethanol exposure. (G–K) Expression of *CDH1* (G), *VIM* (H), *TWIST* (I), and *SNAI1* transcripts (J) and densitometric quantification of E-Cadherin protein levels (K) in BeWO cytotrophoblasts following HE_a miRNAs or control hairpin inhibitor transfection with or without concomitant 320 mg/dl ethanol exposure. Results are expressed as the mean \pm SEM, LDR = molecular weight ladder, $n = 10$ samples per group; ANOVA: significant main effect of HE_a miRNA transfection (##### $P < 0.0001$), significant interaction effect (HE_a miRNA by 320 mg/dl ethanol, [†††† $P < 0.001$]). For post hoc analysis * $P < 0.05$, ** $P < 0.01$ by Tukey's HSD.

Antagomirs prevent HE_a miRNAs' inhibition of EMT

We next investigated if pretreating cytotrophoblasts with pooled HE_a -miRNA antagomirs could prevent inhibition of the EMT pathway caused by transfecting HE_a miRNA mimics. Pretreatment of cytotrophoblasts with HE_a miRNA antagomirs prevented the elevation in *CDH1* caused by transfection with HE_a miRNA mimics (post hoc Tukey's HSD, $n = 10$ samples per group, $P = 0.004$). Likewise, pre-transfection with HE_a miRNA antagomirs also prevented HE_a miRNA mimic-induced reduction of *SNAI1* and *VIM* expression (post hoc Tukey's HSD, $n = 10$ samples per group, $P = 0.007$ and $P < 0.0001$, respectively) (Fig 6A–D).

As with cytotrophoblasts, pre-transfection with HE_a miRNA antagomirs prevented HE_a miRNA mimic-induced reduction of *VIM*, *SNAI1*, and *SNAI2* expression in extravillous trophoblasts (post hoc Tukey's

HSD, $n = 10$ samples per group, $P < 0.0001$, Fig 6E–H). Thus, our data suggest that pretreating cells with HE_a miRNA antagomirs prevents inhibition of EMT pathway members resulting from transfection with HE_a miRNA mimics in cytotrophoblasts and extravillous trophoblasts.

HE_a miRNAs impair extravillous trophoblast invasion

Functionally, inhibition of the EMT pathway should reduce trophoblast invasiveness. Thus, we performed a transwell invasion assay using HTR8 extravillous trophoblasts transfected with HE_a miRNA mimics and antagomirs. Although ethanol exposure by itself did not impair trophoblast invasion (Fig S6), there was a marginally significant interaction effect between ethanol exposure and HE_a miRNA mimic transfection ($F_{(1,28)} = 3.418$, $P = 0.075$). Thus, a planned

comparison indicated that transfection with $_{HEa}$ miRNA mimics significantly reduced trophoblast invasion in the context of 320 mg/dl ethanol co-exposure, relative to the control mimics ($t(14) = 2.762$, $P = 0.015$), consistent with our data demonstrating $_{HEa}$ miRNAs interfere with the EMT pathway (Fig 7A). Contrastingly, transfecting $_{HEa}$ miRNA antagonists increased invasion in the context of 320 mg/dl ethanol co-exposure, although this effect was only marginally significant ($t(14) = 1.805$, $P = 0.093$, Fig 7B).

$_{HEa}$ miRNAs retard trophoblast cell cycle progression

Given the proliferative nature of cytotrophoblasts and the intimate relationship between EMT and cell cycle (64, 65), we assessed the

effects of ethanol and $_{HEa}$ miRNAs on BeWO cytotrophoblast cell cycle. After pulse-labeling the cells with the nucleic acid analog, EdU, for 1-h, we found that individually transfecting six of the $_{HEa}$ miRNA mimics increased EdU incorporation (unpaired t test, $P < 0.05$, false discovery rate [FDR] correction), suggesting an overall increased rate of DNA synthesis (Fig S7A). Contrastingly, simultaneous transfection of $_{HEa}$ miRNAs significantly reduced EdU incorporation ($F_{(1,26)} = 59.69$, $P < 0.0001$), mirroring the effects of increasing concentrations of ethanol ($R^2 = 0.304$, $P = 0.012$) (Fig S7B and A).

Consistent with the increased rates of DNA synthesis resulting from individual $_{HEa}$ miRNA mimic transfection, individual transfection of $_{HEa}$ miRNAs antagonists generally reduced EdU incorporation, although only the antagonist to hsa-miR-760 did so

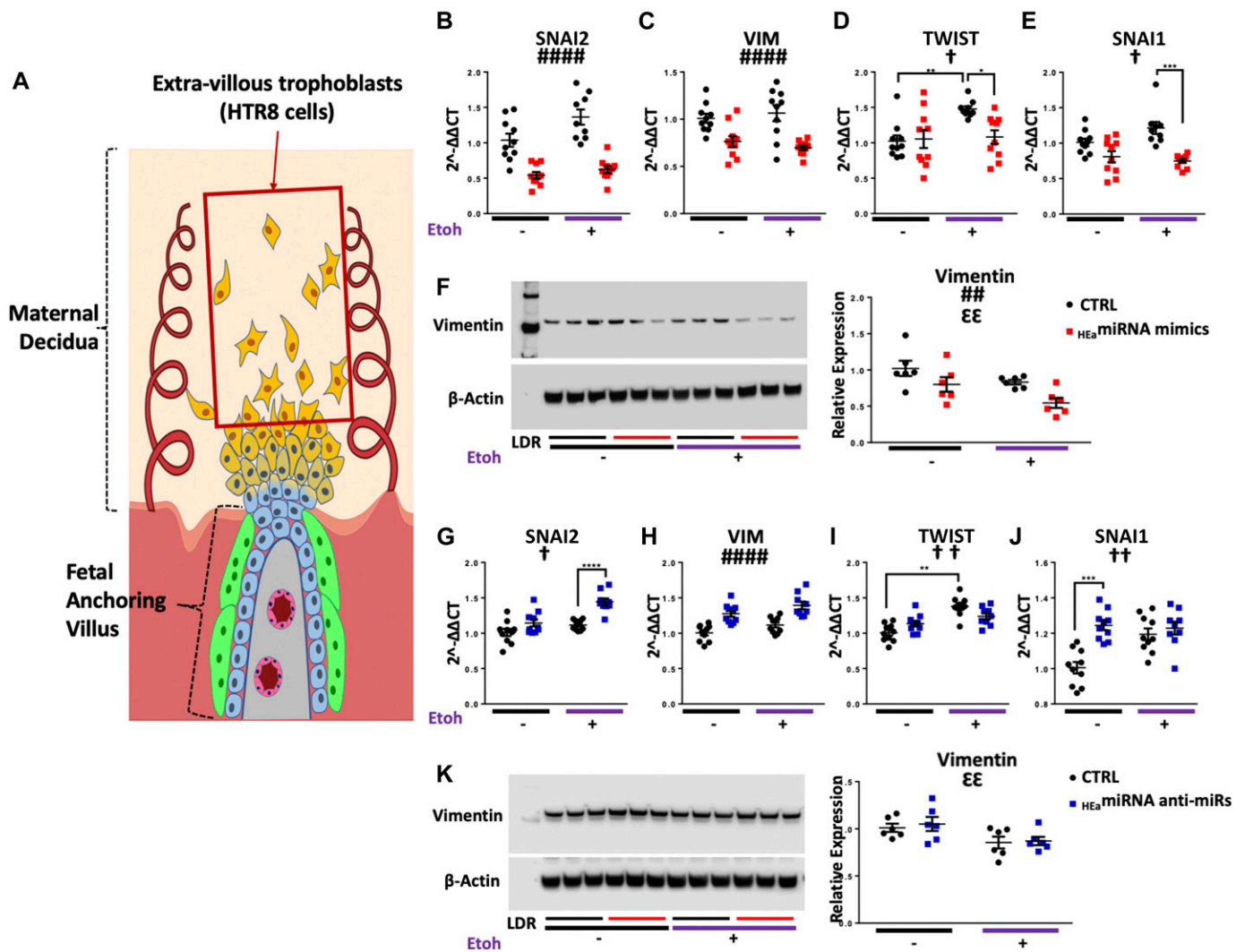


Figure 5. $_{HEa}$ miRNAs interfere with the EMT pathway in HTR8 extravillous trophoblasts.

(A) Diagram of a placental anchoring villous and maternal decidua with the boxed area denoting extravillous trophoblasts. (B–F) Expression of *SNAI2* (B), *VIM* (C), *TWIST* (D), and *SNAI1* transcripts (E) as well as densitometric quantification of vimentin protein levels (F) in HTR8 extravillous trophoblasts following $_{HEa}$ miRNAs or control miRNA overexpression with or without concomitant 320 mg/dl ethanol exposure. (G–K) Expression of *SNAI2* (G), *VIM* (H), *TWIST* (I), and *SNAI1* transcripts (J) as well as densitometric quantification of vimentin protein levels (K) in HTR8 extravillous trophoblasts following $_{HEa}$ miRNA or control hairpin inhibitor transfection with or without concomitant 320 mg/dl ethanol exposure. Results are expressed as the mean \pm SEM, LDR = molecular weight ladder, $n = 10$ samples per group; ANOVA: significant main effect of $_{HEa}$ miRNA transfection ($^{##}P < 0.01$, $^{####}P < 0.0001$), significant main effect of 320 mg/dl ethanol exposure ($^{*E}P < 0.01$), significant interaction effect ($_{HEa}$ miRNA by 320 mg/dl ethanol ($^{*}P < 0.05$, $^{††}P < 0.01$). For post hoc analysis $^{*}P < 0.05$, $^{**}P < 0.01$, $^{***}P < 0.001$, and $^{****}P < 0.0001$ by Tukey's HSD.

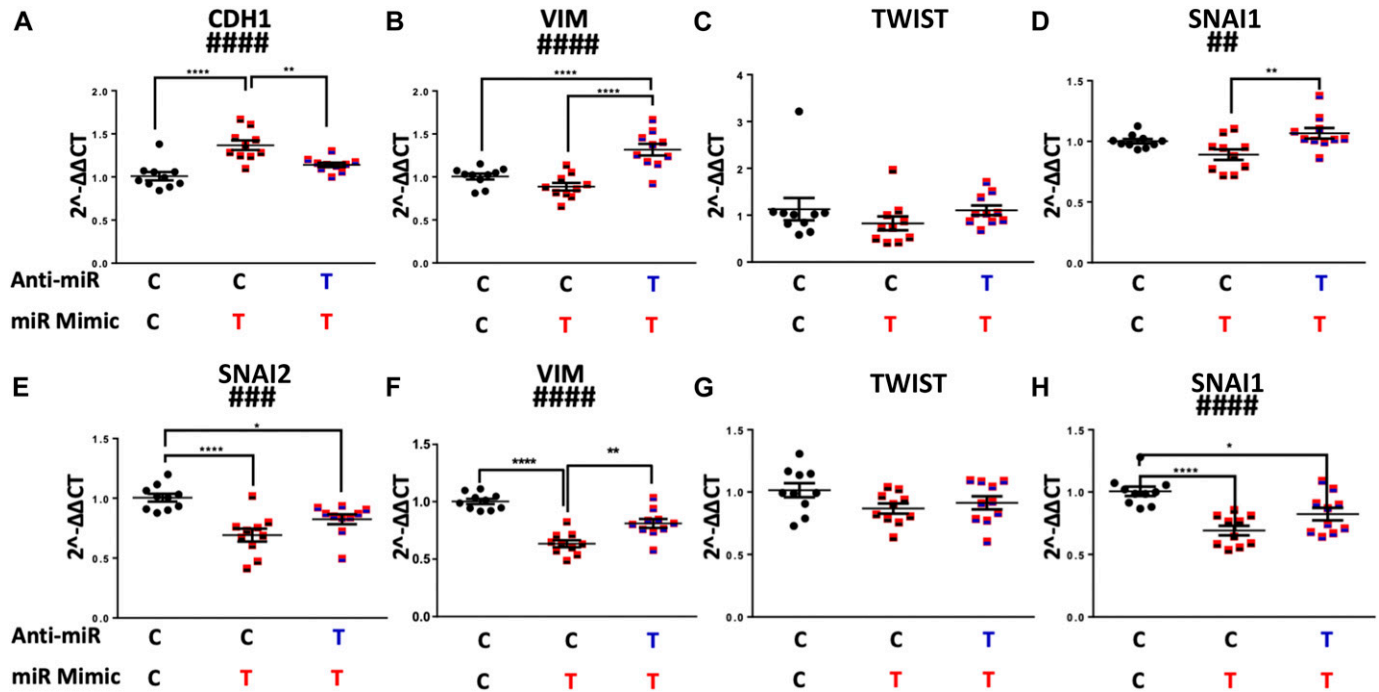


Figure 6. Antagomirs prevent HEa miRNA-induced impairment of EMT. (A–D) Expression of *CDH1* (A), *VIM* (B), *Twist* (C), and *SNAI1* transcripts (D) following control or HEa miRNA hairpin inhibitor transfection followed by control or HEa miRNA overexpression in BeWO cytotrophoblasts. (E–H) Expression of *CDH1* (E), *VIM* (F), *Twist* (G), and *SNAI1* transcripts (H) following control or HEa miRNA antagomir transfection followed by control or HEa miRNA overexpression in HTR8 extravillous trophoblasts. In subheadings, ‘C’ denotes control miRNA mimic or hairpin, whereas ‘T’ denotes HEa miRNA mimic or hairpin inhibitor. Results are expressed as the mean ± SEM, n = 10 samples per group; ANOVA: significant treatment effect (###*P* < 0.01, ####*P* < 0.001, #####*P* < 0.0001). For post hoc analysis, **P* < 0.05, ***P* < 0.01, ****P* < 0.001, *****P* < 0.0001 by Tukey’s HSD.

significantly ($t(110) = 3.059, P = 0.003$, FDR correction) (Fig S7A). Interestingly, simultaneous administration of antagomirs also reduced EdU incorporation, as observed with the pooled HEa miRNA mimics ($F_{(1,26)} = 34.83, P = 0.0005$, Fig 8B).

To further characterize the coordinated effect of HEa miRNAs on cytotrophoblast cell cycle, we pulse-labeled the cells with EdU for 1-h and, post-fixation, labeled them with 7AAD to segregate cells into three groups: G₀/G₁ (7AADlow, EDU-), S (EDU+), and G₂/M (7AADhigh, EDU-). Both 120 mg/dl and 320 mg/dl ethanol exposures significantly decreased the proportion of cells in the S-phase, whereas 320 mg/dl exposure increased the proportion of cells in the G₂/M-phase, consistent with the observed reduction in the rate

of DNA synthesis (Fig S7C). Similar to the effects of ethanol exposure, pooled HEa miRNA mimic administration also significantly decreased the proportion of cells in the S-phase ($F_{(1,28)} = 52.78, P < 0.0001$), whereas increasing the proportion of cells the G₂/M-phase ($F_{(1,28)} = 8.395, P = 0.007$) and exacerbated alcohol’s effects on the cell cycle (Fig 8C). Interestingly, pooled HEa miRNA antagomir administration also reduced the proportion of cells in the S-phase ($F_{(1,26)} = 14.98, P = 0.0007$) and increased the proportion of those in the G₂/M-phase ($F_{(1,26)} = 12.38, P = 0.002$) (Fig 8D).

As with our EMT gene expression data, pretreatment of cytotrophoblasts with HEa miRNA antagomirs prevented further reduction in the rate of DNA synthesis, or cell cycle retardation, that

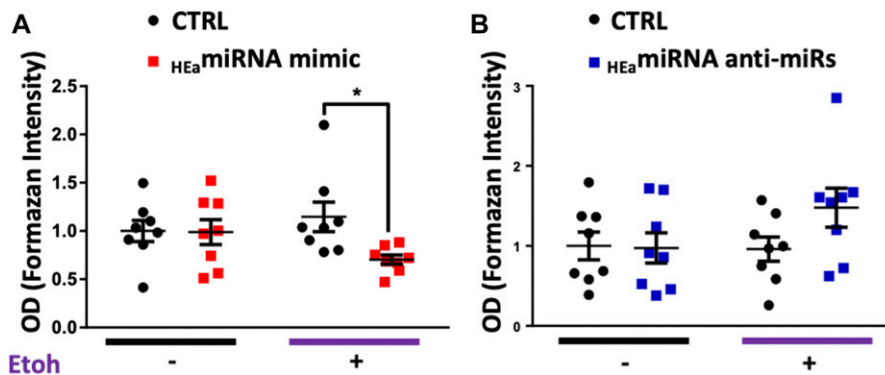


Figure 7. HEa miRNAs impair extravillous trophoblast invasion.

(A, B) Transwell invasion of HTR8 extravillous trophoblasts following transfection with (A) HEa miRNA mimics or (B) hairpin inhibitors with or without concomitant 320 mg/dl ethanol exposure. OD = optical density; results are expressed as the mean ± SEM; n = 10 samples per group; **P* < 0.05 by unpaired t test.

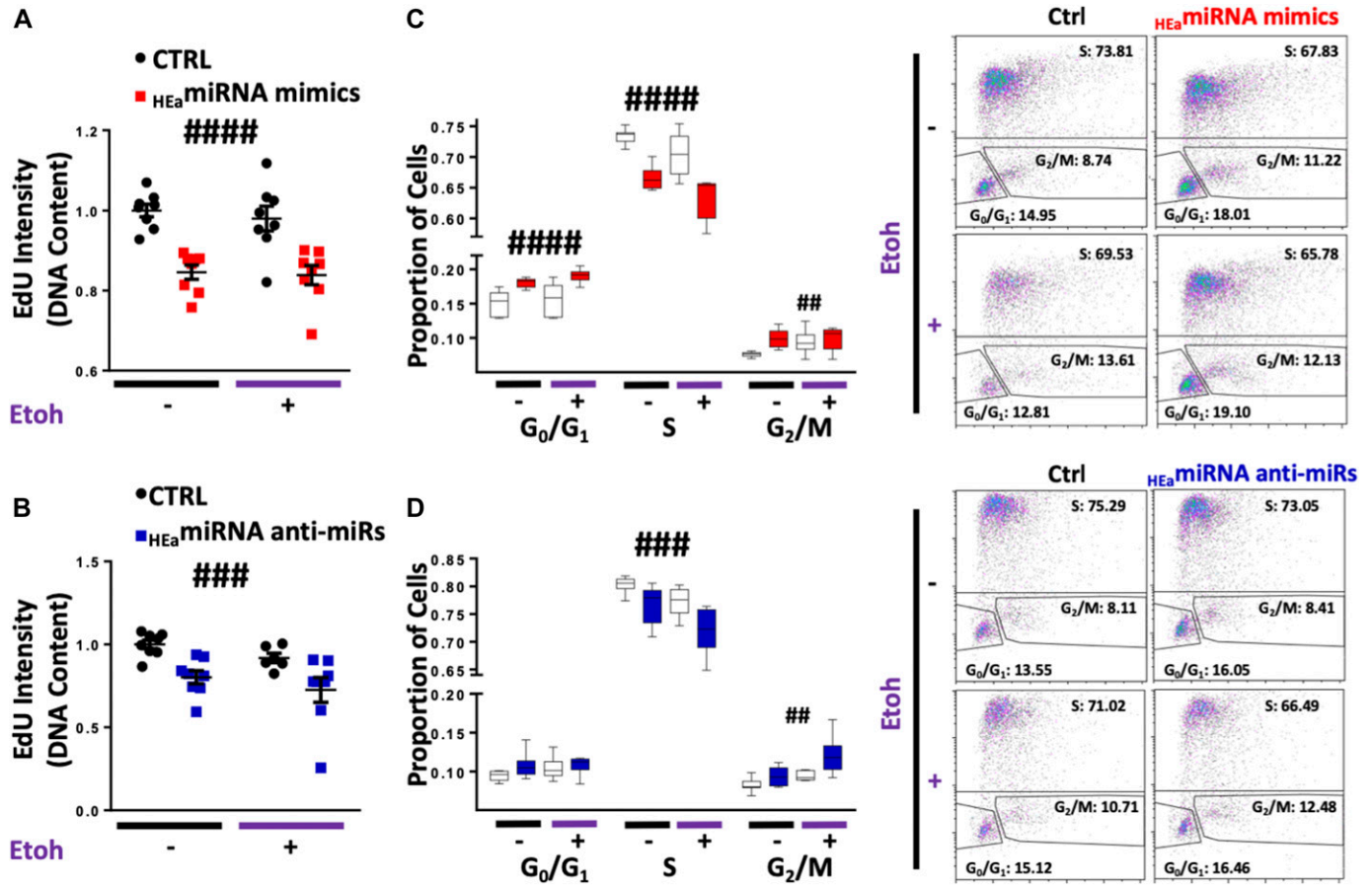


Figure 8. HEAmiRNAs cause cell cycle retardation in trophoblasts.

(A) Degree of EdU incorporation following control and HEAmiRNA overexpression. (B) Degree of EdU incorporation following control and HEAmiRNA hairpin inhibitor transfection. (C) Box and whisker plot for the proportion of cells in the G₀/G₁, S, or G₂/M phase of the cell cycle following control and HEAmiRNA overexpression. (D) Box and whisker plot for the proportion of cells in the G₀/G₁, S, or G₂/M phase of the cell cycle following control and HEAmiRNA hairpin inhibitor transfection with or without concomitant 320 mg/dl ethanol exposure. For box and whisker plots, bounds of box demarcate limits of the first and third quartile, the line in middle is the median, and whiskers represent the range of data. Representative flow cytometry experiment images are shown on the right. n = 10 samples per group; ANOVA: significant main effect of HEAmiRNA transfection (###*P* < 0.01, ####*P* < 0.001, and #####*P* < 0.0001).

would result from transfection with pooled HEAmiRNA mimics (Fig 9A and B).

HEAmiRNAs have minimal effect on cell survival

We next investigated whether ethanol- and HEAmiRNA-induced changes in cell cycle were related to an increase in cell death. Only the 320 mg/dl dose of ethanol exposure demonstrated a slight, but marginally significant effect, of increasing lytic cell death (*t*(18) = 2.022, *P* = 0.054), although there was no effect on apoptosis (Fig S8A and B). However, the changes in cell cycle following transfection of individual or pooled HEAmiRNA mimics were not mirrored by changes in lytic cell death. Nevertheless, two HEAmiRNAs, hsa-miR-671-5p and hsa-miR-449a, did significantly increase apoptosis (unpaired *t* test, *P* < 0.05, FDR correction) (Fig S8C and D).

Contrastingly, transfection of four HEAmiRNA antagonomirs individually, significantly increased lytic cell death (unpaired *t* test, all *P* < 0.05, FDR correction), with the antagonomir to hsa-miR-491-3p also increasing apoptotic cell death (*t*(14) = 3.383, *P* = 0.004, FDR

correction, Fig S8C and D). Likewise, transfection of pooled HEAmiRNA antagonomirs increased lytic cell death (*F*(_{1,36}) = 11.40, *P* = 0.002) but did not cause increased apoptosis (Fig S8E–H). Taken together, our data suggest that whereas ethanol exposure may increase cytotrophoblast death, increased levels of HEAmiRNAs have minimal effects on cell death, suggesting that their effect on cell cycle and the EMT pathway is independent of any effect on cell survival.

HEAmiRNAs modulate cytotrophoblast differentiation-associated Ca²⁺ dynamics

HEAmiRNAs' effects on EMT pathway member expression, coupled with cell cycle retardation, indicate that HEAmiRNAs influence trophoblast maturation. To model HEAmiRNAs' effect on hormone-producing and calcium-transporting syncytiotrophoblasts (66), we used a well-established protocol of forskolin-induced syncytialization of BeWO cytotrophoblasts (67, 68). As expected, forskolin treatment induced fusion/syncytialization of cytotrophoblasts resulting in a greater average cell size in the forskolin + HEAmiRNA

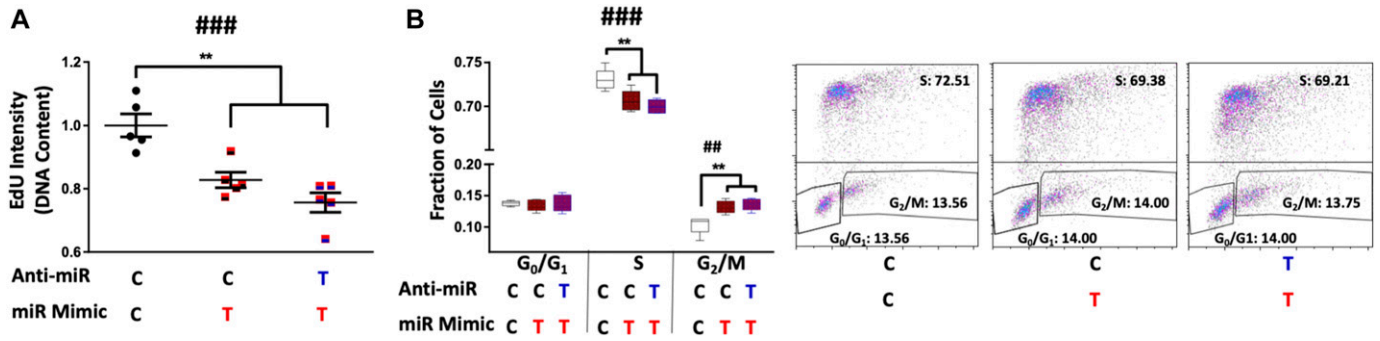


Figure 9. Antagomirs prevent HEA miRNA-induced cell cycle retardation.

(A) Degree of EdU incorporation following control or HEA miRNA hairpin inhibitor transfection followed by control or HEA miRNA overexpression in BeWO cytotrophoblasts. Results are expressed as the mean ± SEM. (B) Box and whisker plot for the proportion of cells in the G₀/G₁, S, or G₂/M phase of the cell cycle following control or HEA miRNA hairpin inhibitor transfection followed by control or HEA miRNA overexpression in BeWO cytotrophoblasts. Bounds of box demarcate limits of the first and third quartile, the line in middle is the median, and whiskers represent the range of data. Representative flow cytometry experiment images are shown on the right. In subheadings, 'C' denotes control miRNA mimic or hairpin, whereas 'T' denotes HEA miRNA mimic or hairpin inhibitor. n = 5 samples per group; ANOVA: significant treatment effect (####P < 0.001). For post hoc analysis, **P < 0.01 by Tukey's HSD.

mimics group ($F_{(1,386)} = 4.386, P = 0.037$). This suggests that the inhibition of EMT by these miRNAs may result in preferential syncytialization instead of differentiation to extravillous trophoblasts (Fig

S9A). Ethanol and forskolin treatment both increased baseline calcium levels, as indicated by the change in fluo-4 fluorescence ($F_{(1,426)} = 5.593$ and 3.665, respectively, $P < 0.0001$, Figs 10A and S9B–D).

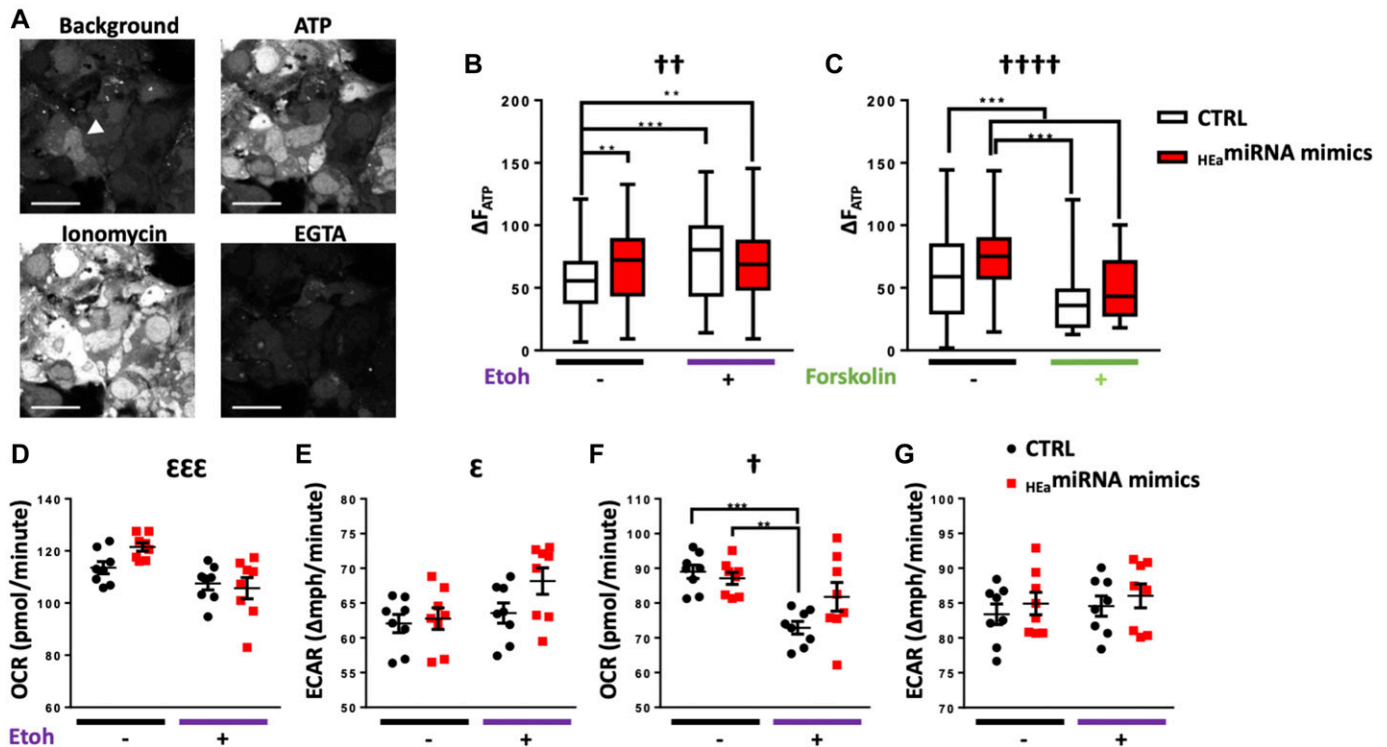


Figure 10. HEA miRNAs modulate differentiation-associated Ca²⁺ dynamics but have minimal effect on the cellular energetics profile.

(A) Time-lapse confocal images of BeWO cytotrophoblasts loaded with fluo-4 Ca²⁺ indicator dye under indicated treatment conditions. The arrowhead indicates a fused, multinuclear cell, scale bar (white) is 50 μ m. (B) Box and whisker plot of intracellular calcium levels following acute ATP administration in BeWO cytotrophoblasts with control and HEA miRNA overexpression with or without concomitant 320 mg/dl ethanol exposure. Bounds of box demarcate limits of the first and third quartile, the line in middle is the median, and whiskers represent the range of data. (C) Box and whisker plot of intracellular calcium levels following acute ATP administration in BeWO cytotrophoblasts with control and HEA miRNA overexpression with or without 20 μ M forskolin treatment. (D–G) Baseline OCR (D), baseline ECAR (E), stressed OCR (F), and stressed ECAR (G) in BeWO cytotrophoblasts with control and HEA miRNA overexpression with or without concomitant 320 mg/dl ethanol exposure. Metabolic stress was induced by treatment with 1 μ M oligomycin and 0.125 μ M FCCP. Results are expressed as the mean ± SEM. n = 10 samples per group; ANOVA: significant main effect of 320 mg/dl ethanol exposure ($^E P < 0.05$, $^{EEE} P < 0.001$), significant interaction effect (HEA miRNA by 320 mg/dl ethanol [$^+ P < 0.05$, $^{++} P < 0.01$, and $^{+++} P < 0.0001$]). For post hoc analysis, *P < 0.05, **P < 0.01, ***P < 0.001, and ****P < 0.0001 by Tukey's HSD.

The effect of ethanol on baseline calcium was abrogated by HEa miRNAs, whereas HEa miRNAs + forskolin was not significantly different to forskolin alone, indicating that forskolin and HEa miRNAs may be affecting similar calcium pathways. The conversion of cytotrophoblasts to syncytiotrophoblasts is accompanied by an increase in endoplasmic reticulum, which could increase calcium-buffering capabilities in response to ethanol stress on the cells; thus, HEa miRNA-induced syncytialization pathways may be protective against ethanol stress.

Adaptations to cellular stress can also be seen in alterations to cellular energetics in response to ethanol, as ethanol-exposed BeWO cells showed decreased baseline and stressed oxygen consumption rates (OCR) ($F_{(1,28)} = 15.55$ and 16.91 , $P = 0.0005$ and 0.0003 , respectively) and increased extracellular acidification rates

(ECAR) ($F_{(1,28)} = 4.868$, $P = 0.036$). However, HEa miRNAs had minimal effects on metabolic activity (Fig 10D–G).

Extracellular ATP has been shown to inhibit trophoblast migration (69) and can directly stimulate increased intracellular calcium elevations through purinergic receptors ubiquitously present on trophoblasts (70). Both HEa miRNA and ethanol administration significantly increased intracellular calcium in response to acute ATP administration ($F_{(1,426)} = 10.34$ and $F_{(1,386)} = 16.30$, $P = 0.001$ and $P < 0.0001$, respectively) (Fig 10B). This may be indicative of a lack of down-regulation of purinergic receptors required in trophoblast migration as part of the interrupted EMT pathway. Forskolin-induced maturation decreased calcium response to ATP ($F_{(1,386)} = 50.72$, $P < 0.0001$) (Fig 10C) and prevented the HEa miRNA-induced increase in ATP response. These data agree with previous studies showing

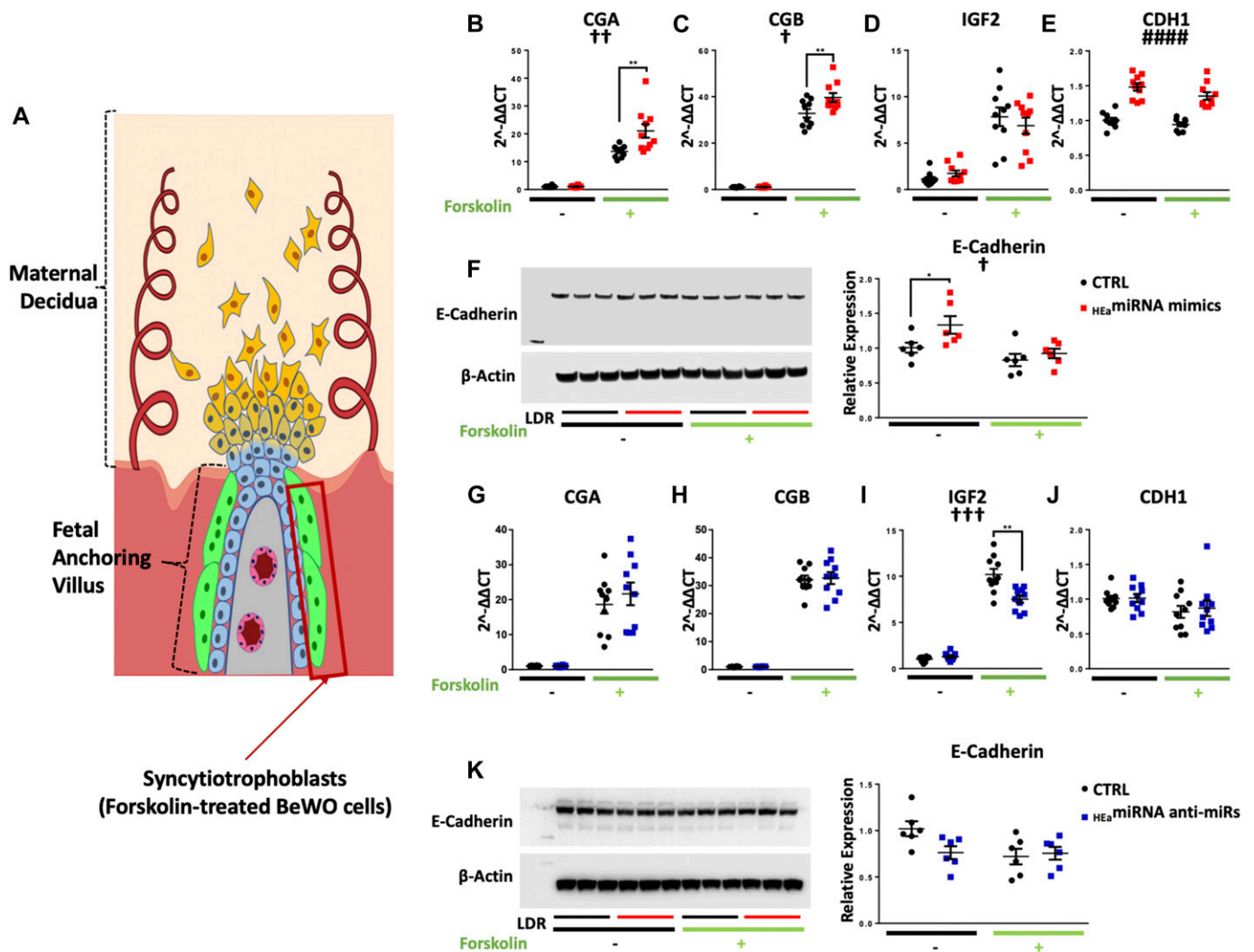


Figure 11. HEa miRNAs promote syncytialization dependent hCG production.

(A) Diagram of a placental anchoring villous and maternal decidua with the boxed area denoting syncytiotrophoblasts. (B–F) Expression of *CGA* (B), *CGB* (C), *IGF2* (D), and *CDH1* transcripts (E) and densitometric quantification of E-Cadherin protein levels (F) in BeWO cytotrophoblasts following HEa miRNAs or control miRNA overexpression with or without $20 \mu M$ forskolin treatment. (G–K) Expression of *CGA* (G), *CGB* (H), *IGF2* (I), and *CDH1* transcripts (J) and densitometric quantification of E-Cadherin protein levels (K) in BeWO cytotrophoblasts following HEa miRNAs or control hairpin inhibitor transfection with or without $20 \mu M$ forskolin treatment. Results are expressed as the mean \pm SEM, LDR = molecular weight ladder, $n = 10$ samples per group; ANOVA: significant main effect of HEa miRNA transfection ($#####P < 0.0001$), significant interaction effect (HEa miRNA by forskolin, $!^*P < 0.05$). For post hoc analysis, $*P < 0.05$, $!^*P < 0.01$ by Tukey's HSD.

increased nuclear trafficking of ionotropic receptor P2X7 and more localized P2X4 expression over placental development, which may decrease the overall calcium influx in response to ATP (71).

HEa miRNAs promote syncytialization-dependent hormone production

Transfection of HEa miRNA mimics did not change *CGA* (encodes Chorionic gonatropin alpha), *CGB* (encodes Chorionic gonadotropin beta), or *IGF2* (encodes Insulin-like growth factor 2) transcript expression relative to the control in non-syncytialized trophoblasts. However, following forskolin-induced syncytialization of BeWO cytotrophoblasts (Fig 11A), HEa miRNA mimics significantly increased expression of *CGA* and *CGB* (post hoc Tukey's HSD, $n = 10$ samples per group, $P = 0.001$ and 0.005 , respectively). Consistent with our previous results, HEa miRNA mimics also increased *CDH1* expression in both cytotrophoblasts and syncytiotrophoblasts ($F_{(1,20)} = 5.286$, $P = 0.032$); there was also a main effect of syncytialization on *CDH1* expression, as has been previously reported ($F_{(1,36)} = 3.391$, $P = 0.034$, Fig 11B–E). Likewise, HEa miRNAs increased E-Cadherin protein expression ($F_{(1,20)} = 5.286$, $P = 0.032$), whereas forskolin decreased it ($F_{(1,20)} = 10.24$, $P = 0.005$) (Fig 11F). On the other hand, there was no effect of HEa miRNA antagonists on *CGA* and *CGB* expression, although we did observe a decrease in *IGF2* transcript expression, following syncytialization, relative to controls (post hoc Tukey's HSD, $n = 10$ samples per group, $P = 0.001$) (Fig 11G–I).

Given that HEa miRNAs promote syncytialization-dependent hormone production, we next investigated maternal plasma levels of intact hCG in our Ukraine birth cohort. Plasma hCG levels were nonsignificantly increased in the second trimester of HEa group mothers relative to their UE counterparts, consistent with previous studies (72). During the third trimester, however, hCG levels remained significantly elevated in HEa group mothers compared with the UE group (median test, $n = 23$ samples in HEa

group and $n = 22$ for HEa and UE groups, $P = 0.03$) (Fig 12). Furthermore, there was no significant difference of gestational age at blood draw between the different groups indicating the increased level of hCG in the HEa group was not confounded by gestational age at which blood was sampled (Fig S10) (73). Interestingly, both alcohol and hCG levels were negatively associated with gestational age at delivery (GAD), with a significant interaction between periconceptional alcohol exposure and hCG levels on GAD (Table S2). Taken together, our data suggest HEa miRNAs may contribute to PAE-dependent increases in hCG levels during pregnancy.

HEa miRNAs reduce fetal growth

To investigate the functional consequences of elevated circulating HEa miRNA levels, we administered miRNA mimics for the eight-mouse homolog HEa miRNAs, or a negative control mimic, through tail vein injection to pregnant mouse dams on GD10. On GD18, growth parameters of male and female fetuses were assessed separately, and data from all same-sex fetuses from a single pregnancy were averaged into one data point. Dams-administered HEa miRNA mimics produced smaller fetuses than those administered control mimics, according to all collected measures of fetal size: fetal weight ($F_{(1,17)} = 9.92$, $P = 0.006$), crown-rump length ($F_{(1,17)} = 9.89$, $P = 0.006$), snout-occipital distance ($F_{(1,17)} = 9.09$, $P = 0.008$), and biparietal diameter ($F_{(1,17)} = 5.99$, $P = 0.026$) (Fig 13B–E). Interestingly, placental weights were also significantly reduced in mice treated with HEa miRNA mimics ($F_{(1,17)} = 6.92$, $P = 0.018$) (Fig 13F).

Following tail vein administration of two human-specific sentinel miRNAs, miR-518f-3p and miR-519a-3p, we found a high bio-distribution of both miRNAs in the placenta, comparable with levels seen in the liver and spleen (Fig S11A and B). Thus, to determine whether HEa miRNA's effects on fetal growth could result from their actions on the placenta, we quantified the placental expression of core EMT members in the GD18 placentas of control and HEa miRNA fetuses. HEa miRNA administration significantly reduced expression of mesenchymal-associated transcript *VIM* ($F_{(1,14)} = 14.23$, $P = 0.002$) and *SNAI2* ($F_{(1,14)} = 5.99$, $P = 0.028$) with a significant sex by HEa miRNA interaction effect on *SNAI1* ($F_{(1,66)} = 5.55$, $P = 0.034$) and *CDH1* ($F_{(1,14)} = 6.01$, $P = 0.028$) (Fig 14A–E). Interestingly, and in line with our in vitro findings whereby HEa miRNAs promoted syncytialization-dependent cell fusion and hCG production, HEa miRNA administration significantly increased expression of the mRNA transcript for *SynB*, a gene that is important for syncytiotrophoblast maturation ($F_{(1,66)} = 4.11$, $P = 0.047$) (Fig 14F).

Discussion

We previously reported that gestational elevation of 11 maternal plasma miRNAs predicted which PAE infants would exhibit adverse outcomes at birth (8). These HEa miRNAs were elevated throughout mid and late-pregnancy, encompassing critical periods for fetal development, and were predicted to target the EMT pathway (8). In this study, we tested this prediction by adopting rodent and macaque gestational moderate alcohol self-administration paradigms. Despite differences in their placental anatomy (74, 75, 76, 77),

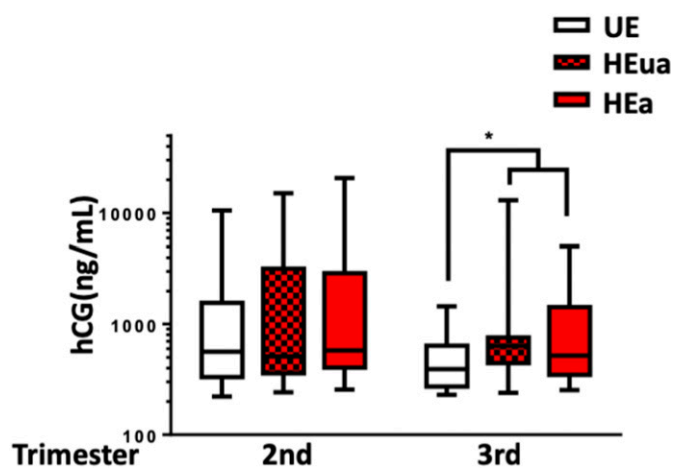


Figure 12. PAE elevates third trimester maternal hCG. Box and whisker plot of the second and third trimester maternal hCG levels in UE, HEua, and HEa group mothers of our Ukrainian birth cohort. Bounds of box demarcate limits of the first and third quartile, the line in middle is the median, and whiskers represent the range of data. Results are expressed as the mean \pm SEM, $n = 22$ – 23 samples per group; * $P = 0.03$ (Mood's median test, $\chi^2 = 7.043$, $df = 2$).

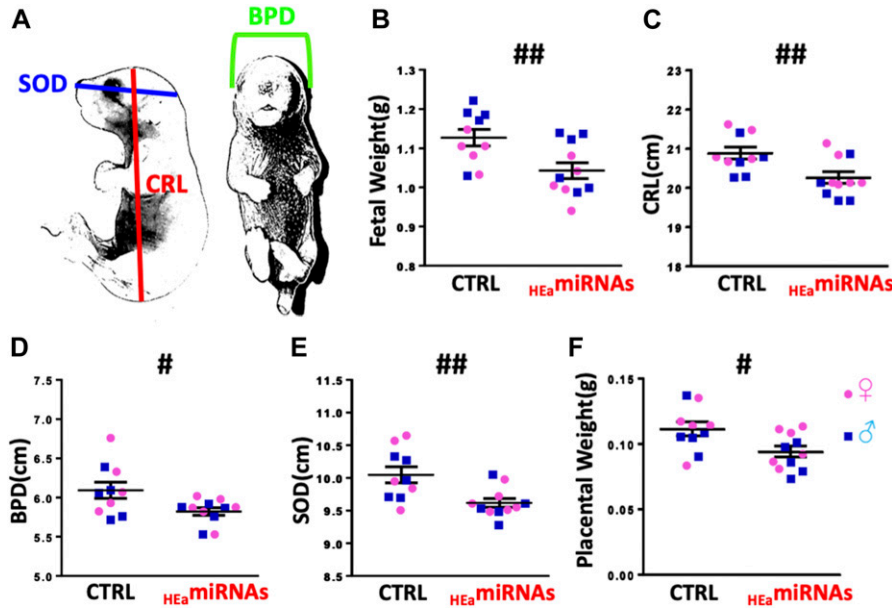


Figure 13. HEAmiRNAs restrict fetal growth. (A) Schematic for measures of crown rump length (CRL), biparietal diameter (BPD), and snout-occipital distance (SOD). (B–F) Fetal weight (B), crown-rump length (C), biparietal diameter (D), snout-occipital distance (E), and placental weight (F) at GD18 following administration of control (Ctrl) and HEAmiRNA mimics to pregnant C57/Bl6 dams on GD10. Dots represent median measures of fetal size and placental weights from male and female offspring in independent litters. There were no significant differences in litter sizes (Ctrl: 8.2 and HEAmiRNAs: 8.5) or sex ratios (Ctrl: 0.86 and HEAmiRNAs: 1.21) between treatment conditions ($P > 0.5$ for all measures). Results are expressed as the mean \pm SEM, $n = 5$ –6 separate litters per treatment condition; ANOVA: significant main effect of HEAmiRNA administration ($^{*}P < 0.05$ and $^{##}P < 0.01$).

we are the first to report that PAE impairs placental EMT across species, indicating a conserved effect of PAE on placental development. In addition, we found that HEAmiRNAs collectively, but not individually, mediated the effects of PAE on core EMT pathway members and that, together, they inhibited EMT in human trophoblast culture models. Although we assessed the effects of HEAmiRNAs on core EMT components (10, 14, 15, 59, 60, 61, 62), analysis of their 3' UTRs indicates that these are unlikely to be the direct targets of HEAmiRNA action. Additional studies will be needed to dissect out the signaling networks that connect HEAmiRNAs to the assessed EMT components.

Interestingly, HEAmiRNAs also promoted syncytialization (forskolin)-dependent hCG expression, mirroring the elevation of third trimester

maternal hCG levels in the PAE group within our clinical cohort. This late-gestation elevation of hCG levels may serve as a compensatory mechanism to prevent the preterm birth associated with PAE, as hCG during late gestation is hypothesized to promote uterine myometrial quiescence (78, 79). In support of this hypothesis, we found significant negative associations between both hCG levels and alcohol consumption with GAD. Furthermore, there was a significant interaction between periconceptional alcohol exposure and hCG levels, with higher hCG levels corresponding to a smaller effect of alcohol exposure at conception on GAD, indicating that hCG moderates the effect of alcohol on age at delivery (Table S2).

Since HEAmiRNAs collectively prevented trophoblast EMT, we hypothesized that, as a functional consequence, these maternal

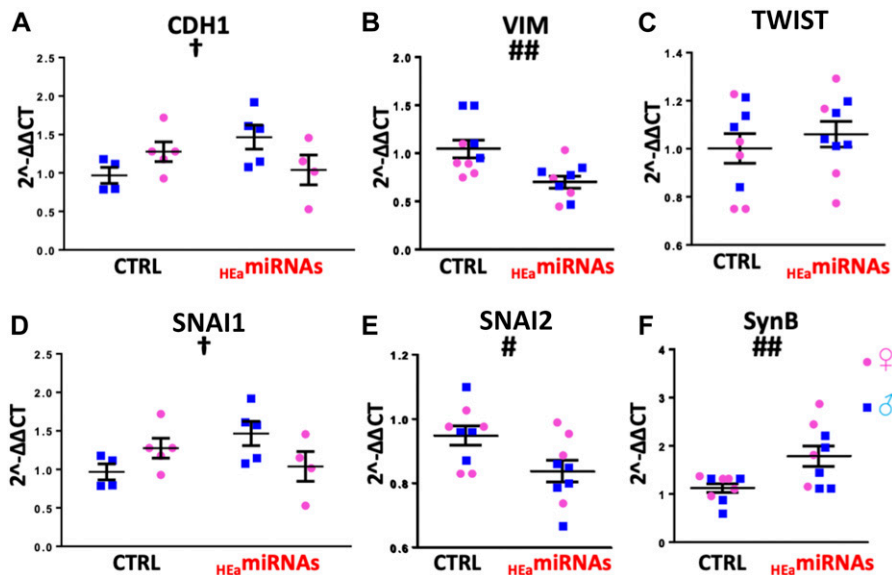


Figure 14. HEAmiRNAs interfere with EMT in the placenta. (A–F) Expression of *CDH1* (A), *VIM* (B), *TWIST* (C), *SNAI1* (D), and *SNAI2* (E) and *SynB* transcripts (F) in GD18 placenta following administration of control (Ctrl) and HEAmiRNA mimics to pregnant C57/Bl6 dams on GD10. Dots represent median expression values of male and female offspring in independent litters. Results are expressed as the mean \pm SEM, $n = 5$ –6 separate litters per treatment condition, ANOVA: significant main effect of HEAmiRNA administration ($^{*}P < 0.05$, $^{##}P < 0.01$), significant interaction effect (fetal sex by HEAmiRNA administration, $^{†}P < 0.05$). For post hoc analysis, $^{*}P < 0.05$ by Tukey's HSD.

miRNAs would also inhibit fetal growth. When we delivered 8 of the 11 $_{\text{HEa}}$ miRNAs known to be present in mouse, to pregnant dams during the period of placental branching morphogenesis and endometrial invasion, and when EMT is particularly active, we found that $_{\text{HEa}}$ miRNAs reduced fetal growth. Importantly, ethanol exposure during this period has also been shown to result in fetal growth deficits and dysmorphia in rodent PAE models (80, 81), suggesting that maternal miRNA-mediated deficits in trophoblast invasion may mediate some of the effects of PAE on fetal growth. In support of this, we found placentas from the $_{\text{HEa}}$ miRNA-treated group had impaired expression of core EMT pathway members. This disruption of placental EMT may also have implications for placental vascular dynamics, as we have also previously observed in mouse models (82). The nonhuman primate tissue analyzed here was also derived from animals that were characterized *in vivo* using MRI and ultrasound imaging, which demonstrated that maternal blood supply to the placenta was lower in ethanol-exposed animals compared with controls and that oxygen availability to the fetal vasculature was reduced (83).

$_{\text{HEa}}$ miRNAs may mediate other pregnancy-associated pathologies, aside from PAE. We identified numerous studies that reported increased circulating and placental levels of at least 8 of 11 $_{\text{HEa}}$ miRNAs in gestational pathologies arising from placental dysfunction. For example, elevated levels of one $_{\text{HEa}}$ miRNA, miR-519a-3p, a member of the placentally expressed C19MC family cluster, was reported in the placentae of patients with preeclampsia, recurrent spontaneous abortion, and intrauterine growth restriction (29, 30, 45, 46). Interestingly, collective overexpression of the 59 C19MC miRNAs inhibits trophoblast migration, explaining their enrichment in the non-migratory villous trophoblasts and suggests their down-regulation is necessary for maturation into invasive extravillous trophoblasts (84). Thus, a greater understanding of the placental roles of $_{\text{HEa}}$ miRNAs may also help disentangle the etiology of other pregnancy complications. We also observed that overexpression of more restricted subsets of $_{\text{HEa}}$ miRNAs associated with preeclampsia, fetal growth restriction, and spontaneous abortion or preterm labor also partly promoted EMT transcript signatures, contrasting with the collective inhibitory action of $_{\text{HEa}}$ miRNAs as a whole. Thus, elevation of some subsets of $_{\text{HEa}}$ miRNAs may constitute a compensatory mechanism aimed at minimizing placental pathologies, although their potential protective effects are masked by the collective elevation of $_{\text{HEa}}$ miRNAs.

Although we did not investigate the effects of PAE on EMT in nonplacental organs, it is likely that PAE broadly disrupts EMT in multiple fetal compartments. Developmental ethanol exposure has been shown to inhibit the EMT-dependent migration of neural crest progenitors involved in craniofacial development, explaining the facial dysmorphology seen in fetal alcohol syndrome and FASDs (85, 86). Outside of its effects on the neural crest, PAE is significantly associated with various congenital heart defects, including both septal defects and valvular malformations (87, 88, 89, 90). Given that development of heart depends on EMT within the endocardial cushions (91, 92), disruption of endocardial EMT could explain both the valvular and septal malformation associated with PAE.

Collectively, our data on $_{\text{HEa}}$ miRNAs suggest miRNA-based interventions could minimize or reverse developmental effects of PAE and other placental-related pathologies. miRNA-based therapeutic

approaches have been advanced for other disease conditions (93, 94). However, our data also suggest the effects of combinations of miRNAs are not a sum of their individual effects. Functional synergy between clusters of co-regulated miRNAs may be a common feature in development and disease. For instance, in 2007, we presented early evidence that ethanol exposure reduced miR-335, -21, and -153 in neural progenitors and that coordinate reduction in these miRNAs yielded net resistance to apoptosis following ethanol exposure (95). In that study, we also showed that coordinate knockdown of these three miRNAs was required to induce mRNA for Jagged-1, a ligand for the Notch cell signaling pathway, an outcome that was not recapitulated by knocking down each miRNA individually (95). More recently, combined administration of miR-21 and miR-146a has been shown to be more effective in preserving cardiac function following myocardial infarction than administration of either of these miRNAs alone (96). Although miRNA synergy has not been explored in detail, these data show that new biology may emerge with admixtures of miRNAs and that therapeutic interventions may require the use of such miRNA admixtures rather than single miRNA molecules, as have been used in clinical studies to date.

In conclusion, we have observed that a set of 11 miRNAs, predictive of adverse infant outcomes following PAE, collectively mediate the effects of alcohol on the placenta. Specifically, elevated levels of these miRNAs together, but not individually, promote an aberrant maturational phenotype in trophoblasts by inhibiting core members of the EMT pathway and promoting cell stress and syncytialization-dependent hormone production. Although extensive research has established circulating miRNAs as biomarkers of disease, our study is one of the first to show how these miRNAs explain and control the disease process themselves. Functionally, we find that these miRNAs are clinically correlated with measures of fetal development and directly cause intrauterine growth restriction when administered *in vivo*. Our work suggests that a greater understanding for the role of $_{\text{HEa}}$ miRNAs during development, and their role in coordinating the EMT pathway in the placenta and other developing tissues, will benefit the understanding of FASDs and other gestational pathologies and potentially lead to effective avenues for intervention.

Materials and Methods

Mouse model of PAE

C57/BL6J mice (The Jackson Laboratory) were housed under reverse 12-h dark/12-h light cycle (lights off at 08:00 h). PAE was performed using a previously described limited access paradigm of maternal drinking (97, 98). Briefly, 60-d-old female mice were subjected to a ramp-up period with 0.066% saccharin containing 0% ethanol (2 d), 5% ethanol (2 d), and finally 10% ethanol for 4-h daily from 10:00 to 14:00 beginning 2 wk before pregnancy, continuing through gestation (Fig S2A). Female mice offered 0.066% saccharin without ethanol during the same time period throughout pregnancy served as controls. Tissue from the labyrinth, junctional, and decidual zone of male and female gestational day 14 (GD14) placentae were

microdissected, snap-frozen in liquid nitrogen, and stored at -80°C preceding RNA and protein isolation.

Mouse model for H_{Ea} miRNA overexpression

For systemic administration of miRNAs, previously nulliparous C57/BL6NHsd dams (Envigo) were tail vein-injected on GD10 with either 50 μg of miRNA miRVana mimic negative control (Cat No. 4464061; Thermo Fisher Scientific) or pooled H_{Ea} miRNA miRVana mimics in In-vivo RNA-LANCER II (3410-01; Bioo Scientific), according to the manufacturer's instructions. The 50 μg of pooled H_{Ea} miRNA mimics consisted of equimolar quantities of mmu-miR-222-5p, mmu-miR-187-5p, mmu-miR-299a, mmu-miR-491-3p, miR-760-3p, mmu-miR-671-3p, mmu-miR-449a-5p, and mmu-miR-204-5p mimics. For biodistribution studies, 50 μg of pooled equimolar quantities of hsa-miR-519a-3p and hsa-miR-518f-3p mimics were injected via tail vein. These human miRNAs were selected because no mouse homologs are known to exist and consequently, estimates for organ distribution of exogenous miRNAs in the mouse are unlikely to be contaminated by the expression of endogenous murine miRNAs. GD10 is a time point near the beginning of the developmental period of branching morphogenesis, immediately following chorioallantoic attachment, during which the placenta invades the maternal endometrium (99). At GD18, pregnancies were terminated with subsequent quantification of fetal weight, crown-rump length, snout-occipital distance, biparietal diameter, and placental weight (Fig 13A). Subsequently, tissue was snap-frozen in liquid nitrogen and stored at -80°C preceding RNA isolation.

Rat model of PAE

Outbred nulliparous Sprague Dawley rats were housed under a 12-h light/12-hour dark cycle. PAE in Sprague Dawley was conducted according to our previously published exposure paradigm (20, 100). Briefly, dams were given a liquid diet containing either 0% or 12.5% ethanol (vol/vol) from 4 d before mating until GD4 (Fig S2B). Dams had ad libitum access to the liquid diet 21 h daily and consumed equivalent calories. Water was offered during the remaining 3 h of the day. On GD5, liquid diets were removed and replaced with standard laboratory chow. On GD20, the placentas were immediately separated into the labyrinth and junctional zone, snap-frozen in liquid nitrogen and stored at -80°C preceding RNA isolation.

Nonhuman primate model of PAE

As previously described in detail (83), adult female rhesus macaques were trained to orally self-administer either 1.5 g/kg/d of 4% ethanol solution (equivalent to six drinks/d) or an isocaloric control fluid before time-mated breeding. Each pregnant animal continued ethanol exposure until gestational day 60 (GD60, term gestation is 168 d in the rhesus macaque) (101). Pregnancies were terminated by cesarean section delivery at three different time points; GD85, GD110, or GD135 (Fig S2C). The macaque placenta is typically bilobed with the umbilical cord insertion in the primary lobe and bridging vessels supplying the fetal side vasculature to the secondary lobe (Fig 2D showing gross placenta anatomy) (102). Full thickness tissue biopsies

(maternal decidua to fetal membranes) were taken from both the primary and secondary lobes of the placenta (Fig 2E showing H&E section of placenta). Samples were immediately snap-frozen in liquid nitrogen and stored at -80°C preceding RNA isolation.

Cell culture trophoblast models

BeWO human cytotrophoblastic choriocarcinoma cells and HTR8/SVneo extravillous cells were sourced from ATCC (Cat No. CCL-98 and CRL-3271, respectively). BeWO cells were maintained in HAM's F12 media containing penicillin (100 U/ml), streptomycin (100 $\mu\text{g}/\text{ml}$), and 10% vol/vol FCS at 37°C and 5% CO_2 . HTR8 cells were maintained in RPMI-1640 media with 5% vol/vol FCS, under otherwise identical conditions. Culture medium was replenished every 2 d and cells subcultured every 4–5 d.

BeWO cells were treated with 20 μM forskolin to induce syncytialization, as previously described (103, 104). BeWO and HTR8 cells were also subjected to four separate ethanol treatment conditions: 0 mg/dl, 60 mg/dl (13 mM), 120 mg/dl (26 mM), or 320 mg/dl (70 mM). To achieve H_{Ea} miRNA overexpression and inhibition, Dharmacon miRIDIAN miRNA mimics and hairpin inhibitors (25 nM), or control mimic (Cat No. CN-001000-01-05; Dharmacon) and hairpin inhibitor (Cat No. CN-001000-01-05; Dharmacon) (25 nM), were transfected into subconfluent BeWO and HTR8 cells using RNAiMAX lipofection reagent (Cat No. 13778; Thermo Fisher Scientific).

Cell cycle analysis

At 48 h post transfection, BeWO cells were pulsed with 10 μM EdU for 1 h. The cells were immediately harvested, and cell cycle analysis was performed with the Click-iT EdU Alexa Fluor 488 Flow Cytometry Assay kit (Cat No. C10420; Thermo Fisher Scientific), in conjunction with 7-amino-actinomycin D (Cat No. 00-6993-50; Thermo Fisher Scientific), according to the manufacturer's instructions, using the Beckman Coulter Gallios 2/5/3 flow cytometer. Data were analyzed using Kaluza software (Beckman Coulter).

Cell death analysis

BeWO cell culture was harvested 48 h post transfection. Media was subjected to lactate dehydrogenase (LDH) detection using the Pierce LDH Cytotoxicity Assay kit (Cat No. 88953; Thermo Fisher Scientific), according to the manufacturer's instructions, for lytic cell death quantification. The Promega Caspase-Glo 3/7 Assay system (Cat No. G8091; Promega) was used to quantify apoptotic cell death.

Invasion assay

At 24 h post-transfection and/or ethanol exposure, HTR8 cells were serum-starved for an additional 18 h. Subsequently, HTR8 cells were seeded onto transwell permeable supports precoated with 300 $\mu\text{g}/\text{ml}$ Matrigel (Cat No. 354248; Corning). After 24 h, cells remaining in the apical chamber were removed with a cotton swab. Cells that invaded into the basal chamber were removed with 1.2 mM 3-(4,5-dimethylthiazol-2-yl)-2,5-diphenyltetrazolium bromide (MTT) for 3 h, and the precipitate solubilized with 10% SDS in

0.01 N HCl. Absorbance intensities were read at 570 nm in a Tecan Infinite 200 plate reader.

Metabolic flux analysis and calcium imaging

BeWO cells (10,000/well) were plated into Seahorse XF96 Cell Culture Microplates (Cat No. 103275-100; Agilent Biotechnology). The OCR, a measure of mitochondrial respiration, and ECAR, a measure of glycolysis, were measured using the Seahorse XFe96 flux analyzer (Seahorse Bioscience). At the time of assay, the cell culture medium was replaced with the appropriate prewarmed Seahorse XF Base Medium (Cat No. 102353-100; Agilent Biotechnology). OCR and ECAR parameters were measured using the Seahorse XFp Cell Energy Phenotype Test kit (Cat No. 103275-100; Agilent Biotechnology). Metabolic stress was induced by simultaneous treatment with 1 μ M oligomycin and 0.125 μ M carbonyl cyanide p-[trifluoromethoxy]-phenyl-hydrazone (FCCP).

BeWO cells were also plated onto glass coverslips in 24-well plates at a density of 30,000 cells/well. After exposure to ethanol and/or forskolin in culture, the cells were prepared for calcium imaging. After replacement of the culture media with external imaging media (154 mM NaCl, 5 mM KCl, 2 mM CaCl₂, 0.5 mM MgCl₂, 5 mM glucose, and 10 mM Hepes, pH 7.4), the cells were loaded for 35 min at 37°C with the calcium indicator dye fluo-4 AM (Cat No. F14201; Thermo Fisher Scientific), at a final concentration of 5 μ M fluo-4 AM in 0.1% DMSO. After incubation, the cells were washed to remove remaining extracellular fluo-4 and imaged at 40 \times using confocal microscopy (FV1200-equipped BX61WI microscope; Olympus Corporation). Time-lapse images were acquired at a frequency of 0.5 Hz. Individual cells were manually outlined, and area and mean fluorescence intensity were obtained for each cell (FIJI image processing package) (105). To determine the functional calcium range of each cell, at the end of imaging, the cells were exposed to 5 μ M ionomycin and 10 mM EGTA (0 mM external Ca²⁺, $F_{\text{range}} = F_{\text{ionomycin}} - F_{\text{EGTA}}$). Baseline fluorescence was determined by averaging the lowest five consecutive fluorescence values during the initial 5 min (F_{baseline}), which was then expressed as a percentage of F_{range} ($\Delta F_{\text{baseline}} = (F_{\text{baseline}} - F_{\text{EGTA}})/F_{\text{range}} \times 100$). Maximal intracellular calcium response to 100 μ M ATP was determined by averaging the highest three consecutive fluorescence values during ATP application (F_{ATP}) and determining the amount of fluorescence as a percentage of F_{range} ($\Delta F_{\text{ATP}} = (F_{\text{ATP}} - F_{\text{EGTA}})/F_{\text{range}} \times 100$).

Quantitative reverse transcriptase–polymerase chain reaction analysis

Total RNA was extracted from tissue, as well as BeWO and HTR8 cells, using the miRNeasy Mini kit (Cat No. 217004; QIAGEN). For miRNA qPCR assays, cDNA was synthesized from 200 ng of total RNA using the miRCURY LNA Universal RT cDNA synthesis kit (Cat No. 203301; Exiqon/Cat No. 339340; QIAGEN), and expression was assessed using miRCURY LNA SYBR Green (Cat No. 203401; Exiqon/Cat No. 339345; QIAGEN). For mRNA qPCR assays, cDNA was synthesized from 500 ng of total RNA using the qScript cDNA Synthesis kit (Cat No. 95047; Quanta/QIAGEN). Gene expression analysis was

performed using PerfeCTa SYBR Green FastMix (Cat No. 95073; Quanta) on the ViiA 7 Real-Time PCR System (Thermo Fisher Scientific). The data presented correspond to the mean $2^{-\Delta\Delta Ct}$ after being normalized to the geometric mean of β -actin, hypoxanthine-guanine phosphoribosyltransferase 1 (HPRT1), and 18s rRNA. Expression data for miRNA was normalized to the geometric mean of miR-25-3p, miR-574-3p, miR-30b-5p, miR-652-3p, and miR-15b-5p. For each primer pair, thermal stability curves were assessed for evidence of a single amplicon, and the length of each amplicon was verified using agarose gel electrophoresis. A list of primers and their sequences is presented in Table S3.

Western immunoblotting analysis

Protein was extracted using 1 \times RIPA lysis buffer (MilliporeSigma) supplemented with Halt Protease Inhibitor Cocktail (Thermo Fisher Scientific). Tissue was homogenized using the Branson Sonifier 150. Protein concentration was determined using Pierce BCA protein assay kit (Thermo Fisher Scientific), and 30 μ g of protein was loaded onto a 4%–12% Bis-Tris (Cat No. NPO323BOX; Invitrogen/Thermo Fisher Scientific), size-fractionated at 200 V for 35 min, and transferred to a PVDF membrane using the iBlot transfer system (Invitrogen/Thermo Fisher Scientific). Blots with protein from cultured cells were blocked with 5% nonfat dry milk in tris-buffered saline containing Tween-20 (TTBS) for 1 h and incubated overnight with primary antibody. The blot was then washed and incubated with an HRP-conjugated goat anti-rabbit or anti-mouse IgG (Invitrogen) at dilution 1:1,000 for 1-h, then developed using PerkinElmer Western Lightning Plus Chemi ECL (PerkinElmer) and visualized using a CCD camera (Fluorchem Q, Alpha Innotech). Blots with protein from homogenized tissue were dried overnight, rehydrated in methanol, stained with REVERT Total Protein Stain, and developed with the Odyssey CLx Imaging System (LI-COR). Blots were then blocked with Odyssey Blocking Buffer (TBS) for 1 h and incubated overnight with primary antibody. The blot was then washed and incubated with IRDye 800CW secondary antibody (Cat No. 925-32210; LI-COR). The following antibodies were used: β -Actin HRP (Cat No. sc-47778; Santa Cruz Biotechnology); Goat anti-Mouse IgG (H+L) Secondary Antibody, HRP (Cat No. 62-6520; Thermo Fisher Scientific); Goat anti-Rabbit IgG (H+L) Secondary Antibody, HRP (Cat No. 65-6120; Thermo Fisher Scientific); purified Mouse Anti-E-Cadherin (Cat No. 610181; BD Biosciences); and Rabbit anti-vimentin antibody (EPR3776) (Cat No. ab 924647; Abcam). Protein levels were quantified using the densitometric analysis package in FIJI image processing software (105).

ELISA

The second and third trimester maternal plasma samples were collected as part of a longitudinal cohort study conducted in two regions of Western Ukraine as part of the Collaborative Initiative on FASDs (CIFASD.org) between the years 2006 and 2011, as previously reported (8). Plasma, at a 1:1,000 dilution, was subjected to hCG detection using Abcam's intact human hCG ELISA kit (Cat no. ab100533) following the manufacturer's protocol.

Literature review

We conducted a literature review for $_{\text{HEa}}$ miRNAs and their associated gestational pathology using the National Institute of Health's PubMed search interface. For each miRNA, the following search parameters were used:

[*miRX OR miR X OR miRNA X OR miRNAX or miRNX*]
AND MeSH Term

where X represents the miRNA of interest and automatic term expansion was enabled. The following MeSH terms, and related search terms (in brackets), were used: Fetal Growth Retardation (Intrauterine Growth Retardation, IUGR, Intrauterine Growth Restriction, Low Birth Weight, LBW, Small For Gestational Age, SGA), Premature Birth (Preterm Birth, Preterm Birth, Preterm Infant, Premature Infant, Preterm Labor, Premature Labor), Spontaneous Abortion (Early Pregnancy Loss, Miscarriage, Abortion, Tubal Abortion, Aborted Fetus), Pre-Eclampsia (Pre Eclampsia, Pre-eclampsia, Pregnancy Toxemia, Gestational Hypertension, Maternal Hypertension), and Maternal Exposure (Environmental Exposure, Prenatal Exposure). Returned articles were subsequently assessed for relevance.

Secondary analysis of RNA sequencing data

Expression levels of $_{\text{HEa}}$ miRNAs in tissues were determined using the Human miRNA Expression Database and the miRmine Human miRNA expression database (58, 106). For expression analysis of $_{\text{HEa}}$ miRNA pri-miRNAs, RNA sequencing data were used from NCBI's sequence read archive (<https://www.ncbi.nlm.nih.gov/sra>). The accession numbers for the sequence files are uterus (SRR1957209), thyroid (SRR1957207), thymus (SRR1957206), stomach (SRR1957205), spleen (SRR1957203), small intestine (SRR1957202), skeletal muscle (SRR1957201), salivary gland (SRR1957200), placenta (SRR1957197), lung (SRR1957195), liver (SRR1957193), kidney (SRR1957192), heart (SRR1957191), whole brain (SRR1957183), adrenal gland (SRR1957124), bone marrow (ERR315396), colon (ERR315484), adipose tissue (ERR315332), and pancreas (ERR315479). Deep sequencing analysis was conducted using the Galaxy version 15.07 user interface according to the bioinformatics pipeline outlined in Fig S12.

Statistical analyses

Linear regression models were used to estimate associations between infant growth measures and miRNA expression levels, gestational age at blood draw, the interaction between subject-centered miRNA expression level and gestational age at blood draw, and child sex. Spearman correlations between infant growth measures and subject-centered miRNA expression levels were also calculated. Linear regression models were also used to estimate the associations between gestational at birth and log-transformed hCG levels, ethanol intake, the interaction between log-transformed hCG levels and ethanol intake, gestational at blood draw, and child sex. Statistical analysis and graphs were

generated with GraphPad Prism 6 software (GraphPad Software, Inc), SPSS v24, or R version 3.3.1. Results are expressed as the mean \pm SEM or alternatively as box and whisker plots with the bounds of the box demarcating limits of first and third quartile, a median line in the center of the box, and whiskers representing the total range of data. The overall group effect was analyzed for significance using one-way MANOVA, one-way or two-way ANOVA with Tukey's HSD or Dunnett's multiple comparisons post hoc testing when appropriate (i.e., following a significant group effect in one-way ANOVA or given a significant interaction effect between experimental conditions in two-way ANOVA), to correct for a family-wise error rate. A two-tailed *t* test was used for planned comparisons. For experiments characterizing the individual effects of $_{\text{HEa}}$ miRNAs against the control miRNA or antagomirs, individual two-tailed *t* test with 5% FDR correction was applied to account for multiple comparisons. All statistical tests, sample sizes, and post hoc analysis are appropriately reported in the results section. A value of $P < 0.05$ was considered statistically significant and a value of $0.1 < P < 0.05$ was considered marginally significant.

Study approval

Human study protocols were approved by the institutional review boards at the Lviv National Medical University, Ukraine, and the University of California San Diego as well as Texas A&M University in the United States. Research was conducted according to the principles expressed in the Declaration of Helsinki with written informed consent received from participants before inclusion in the study. All rodent experiments were performed in accordance with protocols approved by the University of New Mexico Institutional Animal Care and Use Committee (IACUC), the Texas A&M University IACUC, and the University of Queensland Animal Ethics Committees. All procedures involving nonhuman primate research subjects were approved by the IACUC of the Oregon National Primate Research Center (ONPRC), and guidelines for humane animal care were followed. The ONPRC abides by the Animal Welfare Act and Regulations enforced by the US Department of Agriculture.

Supplementary Information

Supplementary Information is available at <https://doi.org/10.26508/lsa.201800252>.

Acknowledgements

This research was supported by grants from the NIH, P50 AA022534 (AM Allan), U01 AA014835 and the Office of Dietary Supplements (CD Chambers), R24 AA019431 (KA Grant), R01 AA021981 (CD Kroenke), R01 AA024659 (RC Miranda), and F31 AA026505 (AM Tseng). We thank the National Health and Medical Research Council of Australia (KM Moritz) for their support. We thank CIFASD for intellectual support and Megan S Pope and Tenley E Lehman for their assistance in conducting cell culture and animal studies. Data on human subjects are deposited at CIFASD.org, in accordance with NIH data repository guidelines.

Author Contributions

AM Tseng: investigation, methodology, and writing—original draft, review, and editing.

AH Mahnke: investigation, methodology, and writing—review and editing.

AB Wells: formal analysis and writing—review and editing.

NA Salem: methodology and writing—review and editing.

AM Allan: investigation, methodology, and writing—review and editing.

VHJ Roberts: investigation, methodology, and writing—review and editing.

N Newman: investigation, methodology, and writing—review and editing.

NAR Walter: investigation, methodology, and writing—review and editing.

CD Kroenke: investigation, methodology, and writing—review and editing.

KA Grant: investigation, methodology, and writing—review and editing.

LK Akison: investigation, methodology, and writing—review and editing.

KM Moritz: investigation, methodology, and writing—review and editing.

CD Chambers: supervision, investigation, methodology, and writing—review and editing.

RC Miranda: supervision, investigation, methodology, and writing—review and editing.

Conflict of Interest Statement

The authors declare that they have no conflict of interest.

References

- Popova S, Lange S, Probst C, Gmel G, Rehm J (2017) Estimation of national, regional, and global prevalence of alcohol use during pregnancy and fetal alcohol syndrome: A systematic review and meta-analysis. *Lancet Glob Health* 5: e290–e299. doi:10.1016/s2214-109x(17)30021-9
- SAMHSA. *The NSDUH Report: 18 Percent of Pregnant Women Drink Alcohol during Early Pregnancy*. NSDUH Report. 2013.
- Bakhireva LN, Sharkis J, Shrestha S, Miranda-Sohrabji TJ, Williams S, Miranda RC (2017) Prevalence of prenatal alcohol exposure in the state of Texas as assessed by phosphatidylethanol in newborn dried blood spot specimens. *Alcohol Clin Exp Res* 41: 1004–1011. doi:10.1111/acer.13375
- May PA, Chambers CD, Kalberg WO, Zellner J, Feldman H, Buckley D, Kopald D, Hasken JM, Xu R, Honerkamp-Smith G, et al (2018) Prevalence of fetal alcohol spectrum disorders in 4 US communities. *JAMA* 319: 474–482. doi:10.1001/jama.2017.21896
- Roozen S, Peters GJ, Kok G, Townend D, Nijhuis J, Curfs L (2016) Worldwide prevalence of fetal alcohol spectrum disorders: A systematic literature review including meta-analysis. *Alcohol Clin Exp Res* 40: 18–32. doi:10.1111/acer.12939
- Lange S, Rehm J, Anagnostou E, Popova S (2017) Prevalence of externalizing disorders and autism spectrum disorders among children with fetal alcohol spectrum disorder: Systematic review and meta-analysis. *Biochem Cell Biol* 1–11. doi:10.1139/bcb-2017-0014
- Bertrand J, Floyd RL, Weber MK, O’Conner M, Johnson KA, Riley EP, Cohen DE. National task force on fetal alcohol syndrome and fetal alcohol effect. In: *US Department of Health and Human Services*. Atlanta, GA: CDC; 2004.
- Balaraman S, Schafer JJ, Tseng AM, Wertelecki W, Yevtushok L, Zymak-Zakutnya N, Chambers CD, Miranda RC (2016) Plasma miRNA profiles in pregnant women predict infant outcomes following prenatal alcohol exposure. *PLoS One* 11: e0165081. doi:10.1371/journal.pone.0165081
- Rossant J, Cross JC (2001) Placental development: Lessons from mouse mutants. *Nat Rev Genet* 2: 538. doi:10.1038/35080570
- E Davies J, Pollheimer J, Yong HEJ, Kokkinos MI, Kalionis B, Knöfler M, Murthi P (2016) Epithelial-mesenchymal transition during extravillous trophoblast differentiation. *Cell Adhes Migration* 10: 310–321. doi:10.1080/19336918.2016.1170258
- Zhou Y, Damsky CH, Fisher SJ (1997) Preeclampsia is associated with failure of human cytotrophoblasts to mimic a vascular adhesion phenotype. One cause of defective endovascular invasion in this syndrome? *J Clin Invest* 99: 2152–2164. doi:10.1172/jci119388
- Damsky CH, Fisher SJ (1998) Trophoblast pseudo-vasculogenesis: Faking it with endothelial adhesion receptors. *Curr Opin Cell Biol* 10: 660–666. doi:10.1016/s0955-0674(98)80043-4
- Brown LM, Lacey HA, Baker PN, Crocker IP (2005) E-cadherin in the assessment of aberrant placental cytotrophoblast turnover in pregnancies complicated by pre-eclampsia. *Histochem Cell Biol* 124: 499–506. doi:10.1007/s00418-005-0051-7
- Fedorova L, Gatto-Weis C, Smali S, Khurshid N, Shapiro JI, Malhotra D, Horrigan T (2012) Down-regulation of the transcription factor snail in the placentas of patients with preeclampsia and in a rat model of preeclampsia. *Reprod Biol Endocrinol* 10: 15. doi:10.1186/1477-7827-10-15
- Blehschmidt K, Mylonas I, Mayr D, Schiessl B, Schulze S, Becker KF, Jeschke U (2007) Expression of E-cadherin and its repressor snail in placental tissue of normal, preeclamptic and HELLP pregnancies. *Virchows Archiv* 450: 195–202. doi:10.1007/s00428-006-0343-x
- Du L, Kuang L, He F, Tang W, Sun W, Chen D (2017) Mesenchymal-to-epithelial transition in the placental tissues of patients with preeclampsia. *Hypertens Res* 40: 67–72. doi:10.1038/hr.2016.97
- Gundogan F, Gilligan J, Ooi JH, Sung J, Qi W, Naram R, de la Monte SM (2013) Dual mechanisms of ethanol-impaired placentation: Experimental model. *J Clin Exp Pathol* 3: 142. doi:10.4172/2161-0681.1000142.
- Tai M, Piskorski A, Kao JCW, Hess LA, M de la Monte S, Gündoğan F (2017) Placental morphology in fetal alcohol spectrum disorders. *Alcohol Alcohol* 52: 138–144. doi:10.1093/alcalc/awg088
- Gundogan F, Gilligan J, Qi W, Chen E, Naram R, de la Monte SM (2015) Dose effect of gestational ethanol exposure on placentation and fetal growth. *Placenta* 36: 523–530. doi:10.1016/j.placenta.2015.02.010
- Gardebjer EM, Cuffe JS, Pantaleon M, Wlodek ME, Moritz KM (2014) Periconceptional alcohol consumption causes fetal growth restriction and increases glycogen accumulation in the late gestation rat placenta. *Placenta* 35: 50–57. doi:10.1016/j.placenta.2013.10.008
- Kalisch-Smith JI, Outhwaite JE, Simmons DG, Pantaleon M, Moritz KM (2016) Alcohol exposure impairs trophoblast survival and alters subtype-specific gene expression in vitro. *Placenta* 46: 87–91. doi:10.1016/j.placenta.2016.08.080
- Bahado-Singh RO, Oz AU, Kingston JM, Shahabi S, Hsu CD, Cole L (2002) The role of hyperglycosylated hCG in trophoblast invasion and the prediction of subsequent pre-eclampsia. *Prenatal Diagn* 22: 478–481. doi:10.1002/pd.329
- Muller F, Savey L, Le Fiblec B, Bussieres L, Ndayizamba G, Colau JC, Giraudet P (1996) Maternal serum human chorionic gonadotropin level

- at fifteen weeks is a predictor for preeclampsia. *Am J Obstet Gynecol* 175: 37–40. doi:[10.1016/S0002-9378\(96\)70247-8](https://doi.org/10.1016/S0002-9378(96)70247-8)
24. Spencer K, Macri JN, Aitken DA, Connor JM (1992) Free beta-hCG as first-trimester marker for fetal trisomy. *Lancet (London, England)* 339: 1480. doi:[10.1016/0140-6736\(92\)92073-o](https://doi.org/10.1016/0140-6736(92)92073-o)
 25. Spencer K (1991) Evaluation of an assay of the free beta-subunit of chorionicadotropin and its potential value in screening for Down's syndrome. *Clin Chem* 37: 809–814.
 26. Salihi HM, Kornosky JL, Lynch O, Alio AP, August EM, Marty PJ (2011) Impact of prenatal alcohol consumption on placenta-associated syndromes. *Alcohol* 45: 73–79. doi:[10.1016/j.alcohol.2010.05.010](https://doi.org/10.1016/j.alcohol.2010.05.010)
 27. Khong TY (2004) Placental vascular development and neonatal outcome. *Semin Neonatal* 9: 255–263. doi:[10.1016/j.siny.2003.11.010](https://doi.org/10.1016/j.siny.2003.11.010)
 28. Ray JG, Vermeulen MJ, Schull MJ, Redelmeier DA (2005) Cardiovascular health after maternal placental syndromes (CHAMPS): Population-based retrospective cohort study. *Lancet (London, England)* 366: 1797–1803. doi:[10.1016/S0140-6736\(05\)67726-4](https://doi.org/10.1016/S0140-6736(05)67726-4)
 29. Wang D, Na Q, Song WW, Song GY (2014) Altered Expression of miR-518b and miR-519a in the placenta is associated with low fetal birth weight. *Am J Perinatol* 31: 729–734. doi:[10.1055/s-0033-1361832](https://doi.org/10.1055/s-0033-1361832)
 30. Wang JM, Gu Y, Zhang Y, Yang Q, Zhang X, Yin L, Wang J (2016) Deep-sequencing identification of differentially expressed miRNAs in decidua and villus of recurrent miscarriage patients. *Arch Gynecol Obstetrics* 293: 1125–1135. doi:[10.1007/s00404-016-4038-5](https://doi.org/10.1007/s00404-016-4038-5)
 31. Hromadnikova I, Kotlabova K, Ondrackova M, Pirkova P, Kestlerova A, Novotna V, Hympanova L, Krofta L (2015) Expression profile of C19MC microRNAs in placental tissue in pregnancy-related complications. *DNA Cell Biol* 34: 437–457. doi:[10.1089/dna.2014.2687](https://doi.org/10.1089/dna.2014.2687)
 32. Hromadnikova I, Kotlabova K, Ivankova K, Krofta L (2017) Expression profile of C19MC microRNAs in placental tissue of patients with preterm prelabor rupture of membranes and spontaneous preterm birth. *Mol Med Rep* 16: 3849–3862. doi:[10.3892/mmr.2017.7067](https://doi.org/10.3892/mmr.2017.7067)
 33. Timofeeva AV, Gusar VA, Kan NE, Prozorovskaya KN, Karapetyan AO, Bayev OR, Chagovets VV, Kliver SF, Iakovishina DY, Frankevich VE, et al (2018) Identification of potential early biomarkers of preeclampsia. *Placenta* 61: 61–71. doi:[10.1016/j.placenta.2017.11.011](https://doi.org/10.1016/j.placenta.2017.11.011)
 34. Dong F, Zhang Y, Xia F, Yang Y, Xiong S, Jin L, Zhang J (2014) Genome-wide miRNA profiling of villus and decidua of recurrent spontaneous abortion patients. *Reproduction (Cambridge, England)* 148: 33–41. doi:[10.1530/rep-14-0095](https://doi.org/10.1530/rep-14-0095)
 35. Hu Y, Li P, Hao S, Liu L, Zhao J, Hou Y (2009) Differential expression of microRNAs in the placenta of Chinese patients with severe pre-eclampsia. *Clin Chem Lab Med* 47: 923–929. doi:[10.1515/cclm.2009.228](https://doi.org/10.1515/cclm.2009.228)
 36. Murphy MS, Casselman RC, Tayade C, Smith GN (2015) Differential expression of plasma microRNA in preeclamptic patients at delivery and 1 year postpartum. *Am J Obstet Gynecol* 213: 367. e1–e9. doi:[10.1016/j.ajog.2015.05.013](https://doi.org/10.1016/j.ajog.2015.05.013)
 37. Bidarimath M, Edwards AK, Wessels JM, Khalaj K, Kridli RT, Tayade C (2015) Distinct microRNA expression in endometrial lymphocytes, endometrium, and trophoblast during spontaneous porcine fetal loss. *J Reprod Immunol* 107: 64–79. doi:[10.1016/j.jri.2014.11.004](https://doi.org/10.1016/j.jri.2014.11.004)
 38. Liu XD, Wu X, Yin YL, Liu YQ, Geng MM, Yang HS, Blachier F, Wu GY (2012) Effects of dietary L-arginine or N-carbamylglutamate supplementation during late gestation of sows on the miR-15b/16, miR-221/222, VEGFA and eNOS expression in umbilical vein. *Amino Acids* 42: 2111–2119. doi:[10.1007/s00726-011-0948-5](https://doi.org/10.1007/s00726-011-0948-5)
 39. Baker BC, Mackie FL, Lean SC, Greenwood SL, Heazell AEP, Forbes K, Jones RL (2017) Placental dysfunction is associated with altered microRNA expression in pregnant women with low folate status. *Mol Nutr Food Res* 61. doi:[10.1002/mnfr.201600646](https://doi.org/10.1002/mnfr.201600646)
 40. Gao Y, She R, Wang Q, Li Y, Zhang H (2018) Up-regulation of miR-299 suppressed the invasion and migration of HTR-8/SVneo trophoblast cells partly via targeting HDAC2 in pre-eclampsia. *Biomed Pharmacother* 97: 1222–1228. doi:[10.1016/j.biopha.2017.11.053](https://doi.org/10.1016/j.biopha.2017.11.053)
 41. Sandrim VC, Luizon MR, Palei AC, Tanus-Santos JE, Cavalli RC (2016) Circulating microRNA expression profiles in pre-eclampsia: Evidence of increased mir-885-5p levels. *BJOG* 123: 2120–2128. doi:[10.1111/1471-0528.13903](https://doi.org/10.1111/1471-0528.13903)
 42. Rodosthenous RS, Burris HH, Sanders AP, Just AC, Dereix AE, Svensson K, Solano M, Tellez-Rojo MM, Wright RO, Baccarelli AA (2017) Second trimester extracellular microRNAs in maternal blood and fetal growth: An exploratory study. *Epigenetics* 12: 804–810. doi:[10.1080/15592294.2017.1358345](https://doi.org/10.1080/15592294.2017.1358345)
 43. Martinez-Fierro ML, Garza-Veloz I, Gutierrez-Arteaga C, Delgado-Enciso I, Barbosa-Cisneros OY, Flores-Morales V, Hernandez-Delgadillo GP, Rocha-Pizana MR, Rodriguez-Sanchez IP, Badillo-Almaraz JJ, et al (2018) Circulating levels of specific members of chromosome 19 microRNA cluster are associated with preeclampsia development. *Arch Gynecol Obstet* 297: 365–371. doi:[10.1007/s00404-017-4611-6](https://doi.org/10.1007/s00404-017-4611-6)
 44. Yang S, Li H, Ge Q, Guo L, Chen F (2015) Deregulated microRNA species in the plasma and placenta of patients with preeclampsia. *Mol Med Rep* 12: 527–534. doi:[10.3892/mmr.2015.3414](https://doi.org/10.3892/mmr.2015.3414)
 45. Hromadnikova I, Kotlabova K, Ivankova K, Krofta L (2017) First trimester screening of circulating C19MC microRNAs and the evaluation of their potential to predict the onset of preeclampsia and IUGR. *PLoS One* 12: e0171756. doi:[10.1371/journal.pone.0171756](https://doi.org/10.1371/journal.pone.0171756)
 46. Zhang M, Muralimanoharan S, Wortman AC, Mendelson CR (2016) Primate-specific miR-515 family members inhibit key genes in human trophoblast differentiation and are upregulated in preeclampsia. *Proc Natl Acad Sci USA* 113: E7069–E76. doi:[10.1073/pnas.1607849113](https://doi.org/10.1073/pnas.1607849113)
 47. Nemoto T, Kakinuma Y, Shibasaki T (2015) Impaired miR449a-induced downregulation of Crhr1 expression in low-birth-weight rats. *J Endocrinol* 224: 195–203. doi:[10.1530/joe-14-0537](https://doi.org/10.1530/joe-14-0537)
 48. Mei Z, Huang B, Mo Y, Fan J (2017) An exploratory study into the role of miR-204-5p in pregnancy-induced hypertension. *Exp Ther Med* 13: 1711–1718. doi:[10.3892/etm.2017.4212](https://doi.org/10.3892/etm.2017.4212)
 49. Choi SY, Yun J, Lee OJ, Han HS, Yeo MK, Lee MA, Suh KS (2013) MicroRNA expression profiles in placenta with severe preeclampsia using a PNA-based microarray. *Placenta* 34: 799–804. doi:[10.1016/j.placenta.2013.06.006](https://doi.org/10.1016/j.placenta.2013.06.006)
 50. Kaufmann P, Black S, Huppertz B (2003) Endovascular trophoblast invasion: Implications for the pathogenesis of intrauterine growth retardation and preeclampsia. *Biol Reprod* 69: 1–7. doi:[10.1095/biolreprod.102.014977](https://doi.org/10.1095/biolreprod.102.014977)
 51. Barrientos G, Pussetto M, Rose M, Staff AC, Blois SM, Toblli JE (2017) Defective trophoblast invasion underlies fetal growth restriction and preeclampsia-like symptoms in the stroke-prone spontaneously hypertensive rat. *Mol Hum Reprod* 23: 509–519. doi:[10.1093/molehr/gax024](https://doi.org/10.1093/molehr/gax024)
 52. Roberts JM, Escudero C (2012) The placenta in preeclampsia. *Pregnancy Hypertens* 2: 72–83. doi:[10.1016/j.preghy.2012.01.001](https://doi.org/10.1016/j.preghy.2012.01.001)
 53. Fisher SJ (2015) Why is placentation abnormal in preeclampsia? *Am J Obstet Gynecol* 213: S115–S22. doi:[10.1016/j.ajog.2015.08.042](https://doi.org/10.1016/j.ajog.2015.08.042)
 54. Crosley EJ, Elliot MG, Christians JK, Crespi BJ (2013) Placental invasion, preeclampsia risk and adaptive molecular evolution at the origin of the great apes: Evidence from genome-wide analyses. *Placenta* 34: 127–132. doi:[10.1016/j.placenta.2012.12.001](https://doi.org/10.1016/j.placenta.2012.12.001)
 55. Lyall F, Bulmer JN, Duffie E, Cousins F, Theriault A, Robson SC (2001) Human trophoblast invasion and spiral artery transformation: The role of PECAM-1 in normal pregnancy, preeclampsia, and fetal growth restriction. *Am J Pathol* 158: 1713–1721. doi:[10.1016/S0002-9440\(10\)64127-2](https://doi.org/10.1016/S0002-9440(10)64127-2)
 56. Goldman-Wohl D, Yagel S (2002) Regulation of trophoblast invasion: From normal implantation to pre-eclampsia. *Mol Cell Endocrinol* 187: 233–238. doi:[10.1016/S0303-7207\(01\)00687-6](https://doi.org/10.1016/S0303-7207(01)00687-6)

57. Balaraman S, Lunde ER, Sawant O, Cudd TA, Washburn SE, Miranda RC (2014) Maternal and neonatal plasma microRNA biomarkers for fetal alcohol exposure in an ovine model. *Alcohol Clin Exp Res* 38: 1390–1400. doi:[10.1111/acer.12378](https://doi.org/10.1111/acer.12378)
58. Panwar B, Omenn GS, Guan Y (2017) miRmine: a database of human miRNA expression profiles. *Bioinformatics* 33: 1554–1560. doi:[10.1093/bioinformatics/btx019](https://doi.org/10.1093/bioinformatics/btx019)
59. Vicovac L, Aplin JD (1996) Epithelial-mesenchymal transition during trophoblast differentiation. *Acta Anatomica* 156: 202–216.
60. Knöfler M, Pollheimer J (2013) Human placental trophoblast invasion and differentiation: A particular focus on wnt signaling. *Front Genet* 4: 190. doi:[10.3389/fgene.2013.00190](https://doi.org/10.3389/fgene.2013.00190)
61. Arimoto-Ishida E, Sakata M, Sawada K, Nakayama M, Nishimoto F, Mabuchi S, Takeda T, Yamamoto T, Isobe A, Okamoto Y, et al (2009) Up-regulation of alpha5-integrin by E-cadherin loss in hypoxia and its key role in the migration of extravillous trophoblast cells during early implantation. *Endocrinology* 150: 4306–4315. doi:[10.1210/en.2008-1662](https://doi.org/10.1210/en.2008-1662)
62. Sun YY, Lu M, Xi XW, Qiao QQ, Chen LL, Xu XM, Feng YJ (2011) Regulation of epithelial-mesenchymal transition by homeobox gene DLX4 in JEG-3 trophoblast cells: A role in preeclampsia. *Reprod Sci* 18: 1138–1145. doi:[10.1177/1933719111408112](https://doi.org/10.1177/1933719111408112)
63. Barrak J, Msheik H, Abou-Kheir W, Daoud G (2016) Assessment of different trophoblast cell lines as in vitro models for placental development. *Placenta* 45: 106. doi:[10.1016/j.placenta.2016.06.157](https://doi.org/10.1016/j.placenta.2016.06.157)
64. Lovisa S, LeBleu VS, Tampe B, Sugimoto H, Vadnagara K, Carstens JL, Wu CC, Hagos Y, Burckhardt BC, Pentcheva-Hoang T, et al (2015) Epithelial-to-mesenchymal transition induces cell cycle arrest and parenchymal damage in renal fibrosis. *Nat Med* 21: 998–1009. doi:[10.1038/nm.3902](https://doi.org/10.1038/nm.3902)
65. Vega S, Morales AV, Ocana OH, Valdes F, Fabregat I, Nieto MA (2004) Snail blocks the cell cycle and confers resistance to cell death. *Genes Dev* 18: 1131–1143. doi:[10.1101/gad.294104](https://doi.org/10.1101/gad.294104)
66. Moreau R, Hamel A, Daoud G, Simoneau L, Lafond J (2002) Expression of calcium channels along the differentiation of cultured trophoblast cells from human term placenta. *Biol Reprod* 67: 1473–1479. doi:[10.1095/biolreprod.102.005397](https://doi.org/10.1095/biolreprod.102.005397)
67. Lu X, He Y, Zhu C, Wang H, Chen S, Lin HY (2016) Twist1 is involved in trophoblast syncytialization by regulating GCM1. *Placenta* 39: 45–54. doi:[10.1016/j.placenta.2016.01.008](https://doi.org/10.1016/j.placenta.2016.01.008)
68. Omata W, Ackerman WEIV, Vandre DD, Robinson JM (2013) Trophoblast cell fusion and differentiation are mediated by both the protein kinase C and A pathways. *PLoS One* 8: e81003. doi:[10.1371/journal.pone.0081003](https://doi.org/10.1371/journal.pone.0081003)
69. Spaans F, Melgert BN, Chiang C, Borghuis T, Klok PA, de Vos P, van Goor H, Bakker WW, Faas MM (2014) Extracellular ATP decreases trophoblast invasion, spiral artery remodeling and immune cells in the mesometrial triangle in pregnant rats. *Placenta* 35: 587–595. doi:[10.1016/j.placenta.2014.05.013](https://doi.org/10.1016/j.placenta.2014.05.013)
70. Karl PI, Chusid J, Tagoe C, Fisher SE (1997) Ca²⁺ flux in human placental trophoblasts. *Am J Physiol* 272: C1776–C1780. doi:[10.1152/ajpcell.1997.272.6.c1776](https://doi.org/10.1152/ajpcell.1997.272.6.c1776)
71. Roberts VH, Waters LH, Powell T (2007) Purinergic receptor expression and activation in first trimester and term human placenta. *Placenta* 28: 339–347. doi:[10.1016/j.placenta.2006.04.007](https://doi.org/10.1016/j.placenta.2006.04.007)
72. Halmesmaki E, Autti I, Granstrom ML, Stenman UH, Ylikorkala O (1987) Estradiol, estriol, progesterone, prolactin, and human chorionic gonadotropin in pregnant women with alcohol abuse. *J Clin Endocrinol Metab* 64: 153–156. doi:[10.1210/jcem-64-1-153](https://doi.org/10.1210/jcem-64-1-153)
73. Edelstam G, Karlsson C, Westgren M, Lowbeer C, Swahn ML (2007) Human chorionic gonadotropin (hCG) during third trimester pregnancy. *Scand J Clin Lab Invest* 67: 519–525. doi:[10.1080/00365510601187765](https://doi.org/10.1080/00365510601187765)
74. Soares MJ, Chakraborty D, Rumi MAK, Konno T, Renaud SJ (2012) Rat placentation: An experimental model for investigating the hemochorial maternal-fetal interface. *Placenta* 33: 233–243. doi:[10.1016/j.placenta.2011.11.026](https://doi.org/10.1016/j.placenta.2011.11.026)
75. Grigsby PL (2016) Animal models to study placental development and function throughout normal and dysfunctional human pregnancy. *Semin Reprod Med* 34: 11–16. doi:[10.1055/s-0035-1570031](https://doi.org/10.1055/s-0035-1570031)
76. Vercruyse L, Caluwaerts S, Luyten C, Pijnenborg R (2006) Interstitial trophoblast invasion in the decidua and mesometrial triangle during the last third of pregnancy in the rat. *Placenta* 27: 22–33. doi:[10.1016/j.placenta.2004.11.004](https://doi.org/10.1016/j.placenta.2004.11.004)
77. Silva JF, Serakides R (2016) Intrauterine trophoblast migration: A comparative view of humans and rodents. *Cell Adhes Migration* 10: 88–110. doi:[10.1080/19336918.2015.1120397](https://doi.org/10.1080/19336918.2015.1120397)
78. Kurtzman JT, Wilson H, Rao CV (2001) A proposed role for hCG in clinical obstetrics. *Semin Reprod Med* 19: 063–068. doi:[10.1055/s-2001-13912](https://doi.org/10.1055/s-2001-13912)
79. Furcron A-E, Romero R, Mial TN, Balancio A, Panaitescu B, Hassan SS, Sahi A, Nord C, Gomez-Lopez N (2016) Human chorionic gonadotropin has anti-inflammatory effects at the maternal-fetal interface and prevents endotoxin-induced preterm birth, but causes dystocia and fetal compromise in mice. *Biol Reprod* 94: 136. doi:[10.1095/biolreprod.116.139345](https://doi.org/10.1095/biolreprod.116.139345)
80. Henderson GI, Hoyumpa AM Jr, McClain C, Schenker S (1979) The effects of chronic and acute alcohol administration on fetal development in the rat. *Alcohol Clin Exp Res* 3: 99–106. doi:[10.1111/j.1530-0277.1979.tb05281.x](https://doi.org/10.1111/j.1530-0277.1979.tb05281.x)
81. O'Leary-Moore SK, Parnell SE, Godin EA, Dehart DB, Ament JJ, Khan AA, Johnson GA, Styner MA, Sulik KK (2010) Magnetic resonance microscopy-based analyses of the brains of normal and ethanol-exposed fetal mice. *Birth Defects Res A Clin Mol Teratol* 88: 953–964. doi:[10.1002/bdra.20719](https://doi.org/10.1002/bdra.20719)
82. Bake S, Tingling JD, Miranda RC (2012) Ethanol exposure during pregnancy persistently attenuates cranially directed blood flow in the developing fetus: Evidence from ultrasound imaging in a murine second trimester equivalent model. *Alcohol Clin Exp Res* 36: 748–758. doi:[10.1111/j.1530-0277.2011.01676.x](https://doi.org/10.1111/j.1530-0277.2011.01676.x)
83. Lo JO, Schabel MC, Roberts VH, Wang X, Lewandowski KS, Grant KA, Frias AE, Kroenke CD (2017) First trimester alcohol exposure alters placental perfusion and fetal oxygen availability affecting fetal growth and development in a non-human primate model. *Am J Obstet Gynecol* 216: 302. e1–e8. doi:[10.1016/j.ajog.2017.01.016](https://doi.org/10.1016/j.ajog.2017.01.016)
84. Xie L, Mouillet J-F, Chu T, Parks WT, Sadvovsky E, Knöfler M, Sadvovsky Y (2014) C19MC MicroRNAs regulate the migration of human trophoblasts. *Endocrinology* 155: 4975–4985. doi:[10.1210/en.2014-1501](https://doi.org/10.1210/en.2014-1501)
85. Smith SM, Garic A, Flentke GR, Berres ME (2014) Neural crest development in fetal alcohol syndrome. *Birth Defects Res C Embryo Today* 102: 210–220. doi:[10.1002/bdrc.21078](https://doi.org/10.1002/bdrc.21078)
86. Kalcheim C (2016) Epithelial-mesenchymal transitions during neural crest and somite development. *Journal Clin Med* 5: 1. doi:[10.3390/jcm5010001](https://doi.org/10.3390/jcm5010001)
87. Yang J, Qiu H, Qu P, Zhang R, Zeng L, Yan H (2015) Prenatal alcohol exposure and congenital heart defects: A meta-analysis. *PLoS One* 10: e0130681. doi:[10.1371/journal.pone.0130681](https://doi.org/10.1371/journal.pone.0130681)
88. Burd L, Deal E, Rios R, Adickes E, Wynne J, Klug MG (2007) Congenital heart defects and fetal alcohol spectrum disorders. *Congenit Heart Dis* 2: 250–255. doi:[10.1111/j.1747-0803.2007.00105.x](https://doi.org/10.1111/j.1747-0803.2007.00105.x)
89. Serrano M, Han M, Brinez P, Linask KK (2010) Fetal alcohol syndrome: Cardiac birth defects in mice and prevention with folate. *Am J Obstet Gynecol* 203: 75. e7–e15. doi:[10.1016/j.ajog.2010.03.017](https://doi.org/10.1016/j.ajog.2010.03.017)
90. Sarmah S, Marrs JA (2013) Complex cardiac defects after ethanol exposure during discrete cardiogenic events in zebrafish: Prevention with folic acid. *Dev Dyn* 242: 1184–1201. doi:[10.1002/dvdy.24015](https://doi.org/10.1002/dvdy.24015)
91. Combs MD, Yutzey KE (2013) Heart valve development: Regulatory networks in development and disease. *Circ Res* 105: 408–421. doi:[10.1161/circresaha.109.201566](https://doi.org/10.1161/circresaha.109.201566)

92. Lin C-J, Lin C-Y, Chen C-H, Zhou B, Chang C-P (2012) Partitioning the heart: Mechanisms of cardiac septation and valve development. *Development (Cambridge, England)* 139: 3277–3299. doi:[10.1242/dev.063495](https://doi.org/10.1242/dev.063495)
93. Janssen HL, Reesink HW, Lawitz EJ, Zeuzem S, Rodriguez-Torres M, Patel K, van der Meer AJ, Patack AK, Chen A, Zhou Y, et al (2013) Treatment of HCV infection by targeting microRNA. *New Engl J Med* 368: 1685–1694. doi:[10.1056/nejmoa1209026](https://doi.org/10.1056/nejmoa1209026)
94. Beg MS, Brenner AJ, Sachdev J, Borad M, Kang YK, Stoudemire J, Smith S, Bader AG, Kim S, Hong DS (2017) Phase I study of MRX34, a liposomal miR-34a mimic, administered twice weekly in patients with advanced solid tumors. *Invest New Drugs* 35: 180–188. doi:[10.1007/s10637-016-0407-y](https://doi.org/10.1007/s10637-016-0407-y)
95. Sathyan P, Golden HB, Miranda RC (2007) Competing interactions between micro-RNAs determine neural progenitor survival and proliferation after ethanol exposure: Evidence from an ex vivo model of the fetal cerebral cortical neuroepithelium. *J Neurosci* 27: 8546–8557. doi:[10.1523/jneurosci.1269-07.2007](https://doi.org/10.1523/jneurosci.1269-07.2007)
96. Huang W, Tian SS, Hang PZ, Sun C, Guo J, Du ZM (2016) Combination of microRNA-21 and microRNA-146a attenuates cardiac dysfunction and apoptosis during acute myocardial infarction in mice. *Mol Ther Nucleic Acids* 5: e296. doi:[10.1038/mtna.2016.12](https://doi.org/10.1038/mtna.2016.12)
97. Brady ML, Allan AM, Caldwell KK (2012) A limited access mouse model of prenatal alcohol exposure that produces long-lasting deficits in hippocampal-dependent learning and memory. *Alcohol Clin Exp Res* 36: 457–466. doi:[10.1111/j.1530-0277.2011.01644.x](https://doi.org/10.1111/j.1530-0277.2011.01644.x)
98. Kajimoto K, Allan A, Cunningham LA (2013) Fate analysis of adult hippocampal progenitors in a murine model of fetal alcohol spectrum disorder (FASD). *PLoS One* 8: e73788. doi:[10.1371/journal.pone.0073788](https://doi.org/10.1371/journal.pone.0073788)
99. Watson ED, Cross JC (2005) Development of structures and transport functions in the mouse placenta. *Physiology (Bethesda)* 20: 180–193. doi:[10.1152/physiol.00001.2005](https://doi.org/10.1152/physiol.00001.2005)
100. Gårdebjer EM, Anderson ST, Pantaleon M, Wlodek ME, Moritz KM (2015) Maternal alcohol intake around the time of conception causes glucose intolerance and insulin insensitivity in rat offspring, which is exacerbated by a postnatal high-fat diet. *FASEB J* 29: 2690–2701. doi:[10.1096/fj.14-268979](https://doi.org/10.1096/fj.14-268979)
101. Grant KA, Leng X, Green HL, Szeliga KT, Rogers LS, Gonzales SW (2008) Drinking typography established by scheduled induction predicts chronic heavy drinking in a monkey model of ethanol self-administration. *Alcohol Clin Exp Res* 32: 1824–1838. doi:[10.1111/j.1530-0277.2008.00765.x](https://doi.org/10.1111/j.1530-0277.2008.00765.x)
102. Carter AM (2007) Animal models of human placentation: A review. *Placenta* 28 Suppl A:S41–S47. doi:[10.1016/j.placenta.2006.11.002](https://doi.org/10.1016/j.placenta.2006.11.002)
103. Orendi K, Gauster M, Moser G, Meiri H, Huppertz B (2010) The choriocarcinoma cell line BeWo: Syncytial fusion and expression of syncytium-specific proteins. *Reproduction (Cambridge, England)* 140: 759–766. doi:[10.1530/rep-10-0221](https://doi.org/10.1530/rep-10-0221)
104. Oh SY, Hwang JR, Lee Y, Choi SJ, Kim JS, Kim JH, Sadovsky Y, Roh CR (2016) Isolation of basal membrane proteins from BeWo cells and their expression in placentas from fetal growth-restricted pregnancies. *Placenta* 39: 24–32. doi:[10.1016/j.placenta.2016.01.001](https://doi.org/10.1016/j.placenta.2016.01.001)
105. Schindelin J, Arganda-Carreras I, Frise E, Kaynig V, Longair M, Pietzsch T, Preibisch S, Rueden C, Saalfeld S, Schmid B, et al (2012) Fiji: An open-source platform for biological-image analysis. *Nat Methods* 9: 676–682. doi:[10.1038/nmeth.2019](https://doi.org/10.1038/nmeth.2019)
106. Gong J, Wu Y, Zhang X, Liao Y, Sibanda VL, Liu W, Guo AY (2014) Comprehensive analysis of human small RNA sequencing data provides insights into expression profiles and miRNA editing. *RNA Biol* 11: 1375–1385. doi:[10.1080/15476286.2014.996465](https://doi.org/10.1080/15476286.2014.996465)



License: This article is available under a Creative Commons License (Attribution 4.0 International, as described at <https://creativecommons.org/licenses/by/4.0/>).